HHS Public Access

Author manuscript

Nat Chem Biol. Author manuscript; available in PMC 2021 February 18.

Published in final edited form as:

Nat Chem Biol. 2021 January ; 17(1): 20–29. doi:10.1038/s41589-020-0604-z.

Bariatric surgery reveals a gut-restricted TGR5 agonist with anti-diabetic effects

Snehal N. Chaudhari[1,#], **David A. Harris**[2,#], **Hassan Aliakbarian**[2], **James N. Luo**[2], **Matthew T. Henke**[1], **Renuka Subramaniam**[2], **Ashley H. Vernon**[2], **Ali Tavakkoli**[2], **Eric G. Sheu**[2,*], **A. Sloan Devlin**[1,*]

[1]Department of Biological Chemistry and Molecular Pharmacology, Harvard Medical School, Boston, MA, USA

[2]Department of Surgery, Brigham and Women's Hospital, Harvard Medical School, Boston, MA, USA

Abstract

Bariatric surgery, the most effective treatment for obesity and type 2 diabetes, is associated with increased levels of the incretin hormone GLP-1 and changes in levels of circulating bile acids. The levels of individual bile acids in the GI tract following surgery, however, have remained largely unstudied. Using UPLC-MS-based quantification, we observed an increase in an endogenous bile acid, cholic acid-7-sulfate (CA7S), in the GI tract of both mice and humans after sleeve gastrectomy. We show that CA7S is a TGR5 agonist that increases *Tgr5* expression and induces GLP-1 secretion. Further, CA7S administration increases glucose tolerance in insulin-resistant mice in a TGR5-dependent manner. CA7S remains gut-restricted, minimizing off-target effects previously observed for TGR5 agonists absorbed into circulation. By studying changes in individual metabolites following surgery, this study has revealed a naturally occurring TGR5 agonist that exerts systemic glucoregulatory effects while remaining confined to the gut.

Introduction

Obesity and type 2 diabetes (T2D) are medical pandemics. Bariatric surgery, in the form of Roux-en-Y gastric bypass or sleeve gastrectomy (SG), is the most effective and lasting treatment for obesity and related comorbidities[1,2]. For a majority of patients, remission is

*Correspondence: esheu@bwh.harvard.edu, sloan_devlin@hms.harvard.edu.
#Co-first author

Author contributions

A.S.D., E.G.S., S.N.C., and D.A.H. conceived the project and designed the experiments. S.N.C. performed the cell culture experiments, BA profiling, and transcriptional analyses and hormone quantifications on mouse tissues and blood. D.A.H. performed the mouse surgeries and the enteral administration in vivo experiments. H.A., R.S., and J.N.L. performed the gavages, OGTTs, and the lentiviral injection experiments. J.N.L. performed the chronic dosing experiments. M.T.H. performed NMR analyses. A.H.V. collected and provided the human samples. S.N.C., D.A.H., E.G.S., and A.S.D. wrote the manuscript. A.T. provided feedback and reviewed the manuscript. All authors edited and contributed to the critical review of the manuscript.

Competing interests

CA7S is a subject of patents held by HMS and BWH on which S.N.C., D.A.H., E.G.S., and A.S.D. are inventors. A.S.D. is a consultant for Kintai Therapeutics and HP Hood. E.G.S. was previously on the scientific advisory board of Kitotech, Inc.

durable and lasts for years post-surgery[1,3]. Changes consistently observed following surgery include increased GLP-1, a circulating incretin hormone, and changes in the systemic bile acid (BAs) repertoire[4]. BAs are cholesterol-derived metabolites that play crucial roles in host metabolism as detergents that aid absorption of lipids and vitamins, and as ligands for host receptors[5]. BAs are implicated in post-SG therapeutic benefits due to their ability to mediate signaling through the G protein-coupled receptor (GPCR) TGR5 (also known as GPBAR1) [6] and the farnesoid X receptor (FXR, also known as NR1H4)[6]. Thus far, research efforts have focused on overall changes in the total BA pool or in levels of conjugated or unconjugated BAs in circulating blood[4,7]. Individual BAs, however, have different binding affinities for nuclear hormone receptors (NhRs) and GPCRs, and thus unique abilities to modulate glucose homeostasis, lipid accumulation, and energy expenditure[5,8]. It is not sufficient, therefore, to limit analyses to whole classes of BAs. Moreover, local activation of receptors in the intestine can affect global metabolic outcomes. In particular, GLP-1 is secreted post-prandially by enteroendocrine L cells in the lower intestine in response to activation of TGR5, a GPCR with a primary role in energy metabolism[9]. GLP-1 stimulates pancreatic insulin release, and both hormones then regulate metabolism systemically[10]. In this work, we sought to identify specific naturally occurring BAs increased in the gut following SG and investigate the role of these compounds as TGR5 ligands and regulators of glucose metabolism. We identified one BA, cholic acid-7-sulfate (CA7S, **1**), whose levels were increased in cecal contents and feces of mice and humans, respectively, after SG. We then determined that CA7S is a gut-restricted TGR5 agonist and GLP-1 secretagogue that improves systemic glucose clearance when administered to diet-induced obese mice in acute and chronic settings.

Results

CA7S is increased in mice and humans post-SG

SG is the most performed bariatric surgery in the US owing to robust metabolic benefits and favorable side-effect profile[11]. Rodent SG models mimic the positive metabolic outcomes observed in humans and are suitable for studying post-surgical outcomes[12]. In this study, SG or sham surgery was performed on insulin-resistant, diet-induced obese (DIO) mice (Fig. 1a). SG mice displayed improved glucose tolerance and insulin sensitivity 4–5 weeks post-surgery compared to shams (Fig. 1b-e). SG mice also showed a reduction in percent body weight compared to shams without differences in food intake between groups (Supplementary Fig. 1a,b). Mice were euthanized six weeks post-surgery after an overnight fast and their tissues were harvested. Consistent with studies involving humans[4], we observed an increase in circulating GLP-1 in SG mice (Fig. 1f). BAs that are known agonists of TGR5 can induce GLP-1 secretion in lower-intestinal L cells[4,9]. We therefore quantified individual BAs in cecal contents of SG and sham mice using Ultra-high Performance Liquid Chromatography-Mass Spectrometry (UPLC-MS) (Fig. 2a, for structures of all BAs in text, figures, Extended Data, and Supplementary Information, see Extended Data Fig. 1). We observed a significant increase in only one BA in cecal contents of SG mice. Based on its mass, this compound appeared to be a monosulfated metabolite of a trihydroxy BA. We purified this compound from pooled extracts of post-SG cecal contents using mass spectrometry-guided semi-preparative HPLC. Using NMR spectroscopy, we identified this

compound as cholic acid-7-sulfate (CA7S) (Fig. 2b,c, Supplementary Fig. 2, Extended Data Fig. 2). CA7S is a sulfated metabolite of cholic acid (CA, **2**), an abundant primary BA in both mice and humans. Sulfation of BAs predominantly occurs in the liver[13]. Consistent with this observation, we found increased levels of CA7S in the liver of SG mice (Fig. 2d). In agreement with previous studies, SG mice displayed increased levels of total circulating BAs (Supplementary Fig. 3)[7]. However, there was no difference in total gut BA levels as measured in cecal contents of post-SG and post-sham mice (Fig. 2c). Several BAs derived from the primary BA chenodeoxycholic acid (CDCA, **3**) were decreased in mouse cecal contents, including lithocholic acid (LCA, **4**), isolithocholic acid (isoLCA, **5**), and CDCA. There was also a decrease in tauro-chenodeoxycholic acid (TCDCA, **6**) and CDCA in mouse liver (Extended Data Fig. 3, Supplementary Fig. 4). Notably, CA7S was the only BA detected whose levels were significantly higher in SG mouse cecal contents and livers.

To determine whether CA7S concentrations were also higher in humans after surgery, we quantified BAs in stool from patients who had undergone SG. We compared a pre-operative to a post-operative stool sample collected from patients a median of 36 days following SG. Remarkably, even though total fecal BA levels were decreased in patients post-SG, fecal CA7S levels were significantly increased (Fig. 2e). Consistent with our results from mouse cecal contents, we observed decreases in the CDCA-derived BAs isoLCA, LCA, and ursodeoxycholic acid (UDCA, **7**). CA, the putative substrate for production of CA7S, was also decreased in patients after surgery (Extended Data Fig. 4). CA7S was the only BA detected whose levels were increased in patients post-SG (Fig. 2e). To our knowledge, this is the first report of a specific BA metabolite that is significantly increased following SG in both mice and human subjects.

CA7S activates TGR5 and induces GLP-1 secretion in vitro

We next determined whether CA7S can activate TGR5 and induce GLP-1 secretion from L cells. Previous work showed that sulfation of natural BAs and synthetic analogs alters their TGR5 agonistic activity[14]. We therefore hypothesized that CA7S possessed altered TGR5 agonism compared to CA. While sulfation at C3 abolishes TGR5 agonist activity of LCA (reported EC_{50} values of 0.03–3.70 μM and >100 μM for LCA and LCA-3-sulfate, respectively), replacement of the C24-carboxylic acid with a C24-sulfate lowers the EC_{50} of CA, CDCA, and UDCA by an order of magnitude[14,15–18]. We therefore hypothesized that the C7-sulfated version of CA, CA7S, might possess different TGR5 agonistic activities than CA, which is a weak agonist of TGR5 (reported EC_{50} of 7.72–27 μM)[14,15,16,19,20]. We examined the activation of human TGR5 by CA7S, CA, or tauro-deoxycholic acid (TDCA, **8**) using a transient transfection assay in human embryonic kidney cells (HEK293T). TDCA is a naturally occurring BA and potent TGR5 agonist[21]. HEK293T cells were cotransfected with a cAMP response element (CRE)-driven luciferase reporter construct and human *TGR5* expression plasmid. CA7S activated human TGR5 in a dose-dependent manner and to a similar extent as TDCA. CA7S also displayed a lower EC_{50} (0.17 μM) than CA (12.22 μM) (Fig. 3a). CA7S falls within the reported EC_{50} range of endogenous TGR5 ligands and is more potent than reported synthetic ligands (Supplementary Table 1).

TDCA is currently one of the most potent, naturally occurring GLP-1 secretagogues known[21]. CA7S induced GLP-1 secretion in human intestinal L cells (NCI-H716) to a similar degree as TDCA in a dose-dependent manner. CA had no effect on GLP-1 secretion (Fig. 3b). CA7S extracted and purified directly from cecal contents of SG mice also induced GLP-1 secretion in vitro (Extended Data Fig. 5a). Furthermore, siRNA-mediated knockdown of TGR5 abolished both CA7S- and TDCA-mediated secretion of GLP-1 (Fig. 3b, Extended Data Fig. 5b). This result indicates that induction of GLP-1 secretion by CA7S requires TGR5. TGR5 agonism also results in elevated intracellular calcium levels.[22] We observed a dose-dependent increase in calcium levels in NCI-H716 cells treated with CA7S (Extended Data Fig. 5c).

The BA repertoire in sham and SG mouse intestines as well as human feces includes molecules previously shown to be agonists of TGR5, including deoxycholic acid (DCA, **9**) (Supplementary Table 1, Extended Data Figs. 3,4)[23,24]. To investigate whether CA7S can induce GLP-1 secretion in the presence of physiologically relevant amounts of DCA measured in human cecal contents[25], we incubated NCI-H716 cells with 200 μM DCA and varying concentrations of CA7S. As expected, adding DCA resulted in an increase in GLP-1 concentration compared to DMSO control (Fig. 3c). However, even when low concentrations of CA7S (0.1 μM) were added, GLP-1 secretion increased compared to DCA alone. Likewise, when NCI-H716 cells were incubated with a physiologically relevant concentration of LCA (150 μM), adding 0.1 μM CA7S resulted in an increase in GLP-1 secretion (Extended Data Fig. 5d). These results indicate that CA7S can increase GLP-1 secretion even in the presence of endogenous TGR5 agonists.

To further test whether CA7S can induce GLP-1 secretion in the complex BA milieu of the gut, we generated in vitro pools of BAs mimicking the average concentrations found in sham and SG mouse cecum and tested their ability to induce GLP-1 secretion. The SG BA pool significantly increased GLP-1 secretion compared to the sham pool (Fig. 3d). The SG pool generated without CA7S, however, did not induce GLP-1 secretion compared to either the sham pool or DMSO control (Fig. 3d). Our results demonstrate that CA7S, a naturally occurring BA metabolite, is a potent TGR5 agonist that can activate this receptor in the presence of other endogenous TGR5 agonists to induce GLP-1 secretion.

CA7S induces TGR5 signaling and gene expression

We next examined the effects of CA7S on *TGR5* expression. Some small molecule agonists of TGR5 can also increase *TGR5* expression[26–29]. To test whether CA7S induces *TGR5* expression in addition to agonizing this receptor, we incubated NCI-H716 cells with 100 μM CA7S and quantified *TGR5* expression. We observed an increase in *TGR5* expression within 2 hours (Fig. 3e). BA derivatives that are FXR agonists or dual FXR/TGR5 agonists induce *TGR5* expression via FXR receptor activation[26,27]. On the contrary, BAs and BA derivatives that are TGR5-specific agonists can induce *TGR5* expression independent of FXR activation[26]. CA7S did not activate endogenous FXR in human intestinal Caco-2 cells at all concentrations tested (Extended Data Fig. 5e), suggesting that CA7S induces *TGR5* expression through an FXR-independent mechanism.

Enteroendocrine L cells that secrete GLP-1 are distributed in the intestinal epithelial monolayer, particularly in the distal gut[30,31]. *TGR5* is expressed apically and basolaterally on these cells[21]. BA-mediated TGR5 agonism leading to GLP-1 secretion has been suggested to occur predominately with basolateral activation of TGR5[21], a process that requires active or passive transport of BAs from the apical to the basolateral side of the intestinal epithelium[21]. However, sulfated BAs are poor substrates for intestinal BA transporters and are poorly absorbed[13,26,27], making apical activation a more likely route of TGR5 engagement by CA7S. To test whether CA7S can activate TGR5 apically, we differentiated a mixture of human intestinal epithelial Caco-2 cells and enteroendocrine cells NCI-H716 into polarized monolayers in a transwell system. These monolayers form a physical and biochemical barrier to the passage of small molecules, thus mimicking the gut epithelium[32,33]. There was no detectable CA7S in the basolateral chamber following apical treatment with 100 μM CA7S, suggesting that CA7S was neither actively nor passively transported to the basolateral side of the monolayer (Fig. 3f). Apical treatment of the monolayer with CA7S led to a significant increase in both GLP-1 secretion and *TGR5* expression (Fig. 3g,h). Addition of CA7S (100 μM) to the basolateral chamber also induced both GLP-1 secretion and *TGR5* expression. However, because CA7S was not transported across the epithelium, basolateral administration of CA7S is likely not relevant to the in vivo mechanism of TGR5 activation. Thus, CA7S is a TGR5 agonist capable of inducing *TGR5* expression and GLP-1 secretion from the apical side of intestinal epithelial cells.

Enteral CA7S induces GLP-1 and reduces blood glucose

We next evaluated the acute anti-diabetic effects of CA7S in vivo. After an overnight fast, DIO mice were administered either CA7S or PBS via duodenal and rectal catheters (Fig. 4a). Administration of 1 mg of CA7S resulted in an average of 2500 pmol/mg wet mass of CA7S in cecal contents, a concentration similar to observed post-SG levels (Fig. 2c, 4b, Supplementary Table 2). CA7S-treated mice displayed increased systemic GLP-1 levels compared to PBS-treated mice within 15 minutes (Fig. 4c). Moreover, CA7S-treated mice exhibited reduced blood glucose levels and increased insulin levels compared to PBS-treated mice (Fig. 4d,e, Extended Data Fig. 5f). Consistent with our in vitro results in L cells, *TGR5* expression was increased in the colon of CA7S-treated mice (Fig. 4f). GLP-1-producing enteroendocrine L cells are known to be enriched in the colon compared to the small intestine[30,31]. *TGR5* expression was not increased in the terminal ileum of CA7S-treated mice (Fig. 4f). Analysis of individual BAs in the cecum, gallbladder, and liver showed no differences in any other detectable BAs in CA7S-treated compared to PBS-treated mice (Extended Data Fig. 6, Supplementary Figs. 5,6). These results suggest that in an acute setting, distal action of CA7S in the GI tract induces systemic glucose clearance and thus ameliorates hyperglycemia.

Oral CA7S administration increases glucose tolerance

To further study the anti-diabetic effects of CA7S, fasted DIO mice were orally gavaged with CA7S (100 mg/kg). Analysis of cecal contents 5 hours post-gavage showed an average accumulation of 15,000 picomol/mg wet mass of CA7S (Fig. 5a), a concentration that is within an order of magnitude of the average in post-SG mice. Analysis of individual BAs in the cecum, gallbladder, and liver showed no differences in any other BAs between the two

groups (Extended Data Fig. 7, Supplementary Figs. 7,8). Systemic GLP-1 levels were increased in CA7S-gavaged mice compared to PBS-treated mice 5 hours post-treatment (Fig. 5b). This result is consistent with the findings from enteral administration and demonstrates that oral CA7S treatment increases circulating GLP-1 for several hours.

We then determined the effect of CA7S on glucose tolerance over time using an oral glucose tolerance test (OGTT). DIO mice were gavaged with CA7S (100 mg/kg) or PBS and then administered an oral glucose bolus 3 hours later. CA7S treatment resulted in an increased rate of blood glucose clearance (Fig. 5c). Moreover, the total and incremental areas under the glucose versus time curves (AUC and iAUC) were decreased in CA7S-treated mice (Fig. 5d). These results demonstrate that CA7S increases blood glucose clearance following oral glucose challenge.

Anti-diabetic effects of CA7S require TGR5

CA7S is a potent inducer of GLP-1 secretion. We therefore sought to determine if the acute anti-diabetic effects of CA7S are dependent on GLP-1. We performed lentiviral shRNA-mediated knockdown of the GLP-1 receptor (*Glp1r*) in vivo. DIO mice were injected intraperitoneally with 5×10^5 shRNA lentiviral particles targeting *Glp1r*. At day 3 post-injection, *Glp1r* expression in the small intestine, heart, and stomach was significantly reduced, and importantly, the *Glp1r* expression was undetectable in the pancreas (Supplementary Fig. 9a). Mice were then gavaged with CA7S (100 mg/kg) or PBS and subjected to an OGTT 3 hours later. For the final timepoint of the glycemic curve (120 min), CA7S-treated mice displayed lower blood glucose than PBS-treated mice. For all other timepoints and for the AUCs, there were no longer significant differences between the groups in the absence of GLP-1R, suggesting that in an acute setting, the systemic glucose clearing-effects of CA7S are partially dependent on the action of GLP-1 (Fig. 5e,f).

Previous studies have shown that SG confers anti-diabetic effects to mice lacking GLP-1R[34]. However, absence of TGR5 attenuates anti-diabetic effects of SG[35]. These results suggest that while GLP-1R is not required for anti-diabetic effects of SG, presence of TGR5 is required. To determine whether the glucose-clearing effects of CA7S are dependent on TGR5, we performed lentiviral shRNA-mediated knockdown of *Tgr5* in vivo. Similar to the *Glp1r* knockdown, DIO mice were injected intraperitoneally with 5×10^5 shRNA lentiviral particles targeting *Tgr5*. At day 3 post-injection, expression of *Tgr5* in the colon, the primary site of action of CA7S, was significantly reduced (Supplementary Fig. 9b). Mice were then gavaged with CA7S (100 mg/kg) or PBS and subjected to an OGTT 3 hours later. In the absence of TGR5, the glycemic curves for CA7S and PBS-treated animals were almost identical, with no differences in the AUC and iAUC metrics (Fig. 5g,h). Together, these data suggest that in an acute setting, the systemic glucose clearing-effects of CA7S require TGR5 (Fig. 5g,h).

Long-term dosing with CA7S confers anti-diabetic effects

To assess the effects of chronic CA7S treatment, DIO mice were gavaged daily with 100 mg/kg CA7S or vehicle (PBS) for 48 days. Long-term oral gavage with CA7S or PBS led to initial weight loss in all groups. There were no differences between groups in percent body

weight change at the end of the experiment or total food intake (Supplementary Fig. 10a,b). On day 48, mice were euthanized following an overnight fast. CA7S gavage led to an accumulation of 30,000 picomol/mg wet mass of this compound in murine cecal contents (mean value, Fig. 6a). CA7S-dosed animals displayed a significant increase in circulating GLP-1 levels (Fig. 6b). Moreover, CA7S-treated mice exhibited reduced blood glucose levels and increased insulin levels compared to PBS-treated mice (Fig. 6c,d, Supplementary Fig. 10c). Thus, CA7S can improve diabetic phenotypes in DIO mice in a weight loss-independent manner. Chronic dosing with CA7S did not alter total levels of BAs in the cecum, gallbladder, or liver (Extended Data Fig. 8, Supplementary Figs. 11,12). However, LCA and UDCA levels were decreased in cecal contents, similar to post-SG (Extended Data Figs. 3,4,8). Chronic CA7S treatment did not alter BA levels in liver or gallbladder, suggesting that BA synthesis was unaffected (Supplementary Figs. 11,12). Consistent with our enteral treatment results, mice dosed chronically with CA7S displayed increased colonic levels of *Tgr5* expression compared to the PBS-dosed mice (Fig. 6e). These results suggest that in a chronic setting, CA7S induces GLP-1 secretion and ameliorates hyperglycemia.

CA7S is gut-restricted and non-toxic

While high concentrations of CA7S were observed in the intestine, this metabolite was undetectable in both circulating and portal venous blood from SG and sham-operated mice (Supplementary Table 2), suggesting that CA7S is neither recycled via enterohepatic circulation nor absorbed into systemic circulation. In contrast, the known endogenous TGR5 agonists TDCA and DCA are found in circulation in mice[8]. Introduction of CA7S via enteral administration or acute or chronic oral gavage resulted in only minor amounts in circulation and portal venous blood (Supplementary Table 2). These findings are consistent with previous observations that sulfated BAs, in particular 7α-sulfated BAs, are poorly absorbed in the intestine[13].

While synthetic TGR5 agonists ameliorate diabetic phenotypes[36], their therapeutic use is hampered by side effects resulting from their absorption into circulation[36,37]. Systemically absorbed TGR5 agonists reduce bile secretion and induce gallbladder filling, thereby causing bile stasis[9,37]. We did not observe any change in gallbladder weight in DIO mice 5 hours post-CA7S gavage compared to PBS treatment (Fig. 6f). In addition, SG did not induce a change in gallbladder weight despite increased CA7S levels (Fig. 6g). There was also no difference in individual BAs or total BA levels in sham versus SG gallbladders (Supplementary Fig. 13). Furthermore, chronic CA7S treatment did not affect gallbladder weight (Fig. 6h). These results suggest that in both acute and chronic settings, CA7S does not display one of the major side-effects of non-gut-restricted TGR5 agonists.

High intestinal BA concentrations can damage the gut epithelium, an effect that can lead to inflammation and disruption of intestinal homeostasis[38]. To determine whether CA7S disrupts gut epithelial barrier integrity, we tested the effect of CA7S on permeability in differentiated Caco-2 cell monolayer in a transwell system (Supplementary Fig. 14). Epithelial permeability was assayed by measuring permeability to fluorescein isothiocyanate-dextran (FITC-D) after apical treatment with 1 mM CA7S for 12 hours. Negligible amounts of CA7S were detected in the basolateral chamber, and there was no

increase in FITC-D permeability, suggesting that CA7S remains gut-restricted and does not affect intestinal epithelial integrity (Supplementary Fig. 14a,b). Furthermore, CA7S did not affect the viability of Caco-2 cells up to 15 mM (Supplementary Fig. 14c), indicating that this metabolite is not toxic to human intestinal cells at physiologically relevant concentrations. In addition, CA7S is stable at physiological pHs (Supplementary Fig. 14d). Together, these results suggest that oral administration of CA7S leads to delivery to the lower intestine without absorption or damage to the intestinal epithelium.

BA analysis following acute and chronic CA7S treatment showed that CA7S administration did not affect the total BA pool, nor did this treatment increase other BAs in the cecum (Extended Data Figs. 6-8, Supplementary Figs. 5-8,11,12). To determine whether CA7S interacts with other host receptors, we screened CA7S against a panel of 19 nuclear hormone receptors and 169 G-protein coupled receptors for agonist and antagonist activities. CA7S did not appreciably agonize or antagonize any receptor tested (Supplementary Note). Therefore, CA7S appears to exert anti-diabetic effects without affecting overall BA synthesis or BA signaling pathways.

Discussion

By quantifying changes in individual BAs, we found that the sulfated metabolite, CA7S, is increased in both the mouse GI tract and human feces following SG. We then found that CA7S is a potent TGR5 agonist that induces the secretion of the incretin hormone, GLP-1 from enteroendocrine L cells both in vitro and in vivo. In acute and chronic settings, we observed that CA7S exhibits anti-diabetic effects, including decreasing blood glucose levels and increasing glucose tolerance in insulin-resistant mice. Unlike known endogenous TGR5 agonists, CA7S is not absorbed into portal or systemic circulation. Moreover, CA7S increased gene expression of its target receptor TGR5 in vitro and in vivo. Our knockdown experiments demonstrated that in an acute setting, TGR5 is necessary for the in vivo efficacy of CA7S.

The finding that CA7S is a novel TGR5 agonist that improves glucose tolerance is noteworthy. CA7S had previously been regarded as a metabolic waste product produced by the liver – a sulfated form of cholic acid that was tagged for excretion in feces[13]. To our knowledge, no role for CA7S as a ligand for a GPCR or NhR has been reported. Our data indicates that CA7S is a signaling molecule that binds to TGR5 exclusively in the gut and increases systemic levels of GLP-1.

CA7S both agonizes and increases the gene expression of TGR5. This dual activity raises the possibility that CA7S may function in vivo through both direct and indirect mechanisms. Therefore, a portion of the anti-diabetic effects of CA7S may occur by upregulation of TGR5 with subsequent TGR5 agonism not only by CA7S but also other abundant, endogenous ligands, including DCA and LCA. Alternative mechanisms of action by CA7S in the presence of high concentrations of other ligands cannot be ruled out. In addition, the mechanism by which CA7S increases *TGR5* expression is currently unknown, as this compound did not agonize FXR in our studies. These questions warrant further study.

Owing to the significant off-target effects caused by TGR5 agonists absorbed into circulation, a gut-restricted TGR5 agonist has been suggested as a potential improved therapeutic for T2D[37]. Our data indicate that CA7S is a gut-restricted TGR5 agonist. CA7S was neither actively nor passively transported across a gut epithelial monolayer, did not disrupt epithelial barrier integrity, and could activate TGR5 apically in vitro. In addition, acute and chronic in vivo administrations led to low to undetectable levels of CA7S in portal and systemic circulation. CA7S does not induce gallbladder filling as has been reported for synthetic TGR5 agonists that enter circulation. Furthermore, CA7S is not toxic to human intestinal cells and is stable at physiological pHs. Additional studies are required to assess the long-term effects of CA7S on weight loss and food intake. Nonetheless, as a result of its beneficial acute metabolic effects, gut restriction, and low toxicity, CA7S could be a candidate for the development of a T2D therapeutic.

The role that CA7S plays in the metabolic changes observed post-SG remains unknown. Due to the redundancy of sulfotransferases (SULTs), the enzymes responsible for hepatic CA7S synthesis[39], knockdown of endogenous CA7S levels may be challenging. If this obstacle could be overcome, performing SG on CA7S-depleted mice would help reveal the contribution of this molecule to the metabolic effects of the surgery. We observed decreases in other BAs post-SG. Levels of CDCA were decreased in mouse cecal contents and liver, levels of UDCA were decreased in human feces post-SG, and levels of LCA and isoLCA were decreased in both mouse cecal contents and human feces. CDCA is an FXR agonist, LCA is a TGR5 agonist, while UDCA is relatively inert toward FXR and TGR5[40]. FXR and TGR5 agonism has been shown to induce metabolic benefits, including increased glucose tolerance[6,35,41]. Thus, decreases in levels of these metabolites post-SG would seem to oppose the anti-hyperglycemic effects of the surgery. Interestingly, we observed similar decreases in CDCA, LCA, and UDCA levels in cecal contents of mice chronically treated with CA7S. Further research may reveal if and how these compounds contribute to metabolic effects post-SG.

Our knockdown studies suggest that the anti-diabetic effects of CA7S are partially dependent on GLP-1R and dependent on TGR5. Our work is consistent with previous studies that have found that absence of TGR5 and not GLP-1R attenuates post-SG anti-diabetic effects[34,35]. These results raise the possibility that GLP-1-independent processes downstream of TGR5 may contribute to the increase in glucose tolerance caused by CA7S. TGR5 is broadly expressed in a variety of cell types, including immune, fat, and liver cells [42]. Future work may elucidate other TGR5-dependent mechanisms through which CA7S exerts its glucose-lowering effects. More broadly, prior to this work, there were no known individual metabolites whose levels were altered by bariatric surgery that could increase blood glucose clearance. Through the identification and study of CA7S, we have uncovered a metabolite that, while restricted to the GI tract, can improve global glucose regulation.

Online Methods

Animals.—11-week, 13-week, and 16-week old diet induced obese, male, C57Bl/6J mice were purchased from Jackson Laboratory (Bar Harbor, ME) for Sham and SG surgeries, enteral CA7S treatment, and all other non-surgical experiments, respectively. Mice are

placed on high fat diet starting at 6 weeks of age at Jackson Laboratories. Upon receipt, animals were housed in a climate-controlled environment with 12 hour light/dark cycles and continued on a high fat diet (HFD, 60% Kcal fat; RD12492; Research Diets, NJ). Animals acclimated for at least 1 week prior to undergoing procedures. Euthanasia was performed in the fasted state to minimize the confounding effects of varying food intake between mice and to allow for accurate fasting glucose and GLP-1 measurements. Animals were cared for according to the American Association for Laboratory Animal Science guidelines.

Sleeve gastrectomy (SG) and sham procedures.—11-week-old DIO mice were weight-matched and either underwent SG or Sham operation after a 1 week acclimation. SG was performed through a 1.5 cm laparotomy under isoflurane anesthesia. The stomach was dissected free from its attachments, the vessels between the spleen and stomach (short gastric vessels) ligated, and a tubular stomach was created by removing 80% of the glandular and 100% of the non-glandular stomach with a linear-cutting surgical stapler. Sham operation consisted of laparotomy, stomach dissection, ligation of short gastric vessels, and manipulation of the stomach along the staple line equivalent. Mice were individually housed thereafter to allow for monitoring of food intake, weight, and behavior. Mice were maintained on Recovery Gel Diet (Clear H_2O, Westbrook, ME) from 1 day prior through 6 days after surgery, HFD was restarted on the morning of post-operative day (POD) 7. Mice were sacrificed 5–7 weeks post-surgery after an overnight fast (17:00 to 07:00).

Functional glucose testing.—After a 4 hour fast (8 am to noon), intraperitoneal glucose tolerance testing (IPGTT) and insulin tolerance testing (ITT) were performed at post-operative week 4 and 5, respectively. During IPGTT, mice received 2 mg/g of intraperitoneal D-Glucose (Sigma-Aldrich, St. Louis, MO). Serum glucose levels were measured from the tail vein at 15, 30, 60, and 120 min with a OneTouch Glucometer (Life technologies, San Diego, CA). ITT was performed by intraperitoneal instillation of 0.6u/kg of regular human insulin (Eli Lily and Company, Indianapolis, IN). Serum glucose was measured at 15, 30, and 60 min. Baseline glucose was measured prior to medication administration.

Body weight and food intake measurements.—Sham and SG-operated mice were individually housed and weighed daily for the first post-operative week and then twice weekly until sacrifice. Food intake was measured twice weekly and daily food intake was calculated by averaging the grams eaten per day over the preceding days. For sham and SG-operated animals, food intake measurements were started on POD 10 as animals were transitioned from Gel to high fat diet on POD 7. For chronic CA7S experiments, mice were weighed and food intake was measured daily until sacrifice.

BA analysis.—BA analyses were performed using a previously reported method[43].

Reagents.: Stock BA solutions were prepared in molecular biology grade DMSO (VWR International, Radnor, PA) and were used to establish standard curves. CA7S was purchased from Caymen Chemicals (Ann Arbor, MI. Cat. No. 9002532). Glyocholic acid (GCA) (Sigma) was used as the internal standard for measurements in mouse tissues.

Extraction.: As previously described[43], cecal, liver, human fecal samples (approximately 50mg each), intact gallbladders, and mouse portal veins were pre-weighed in lysis tubes containing ceramic beads (Precellys lysing kit tough micro-organism lysing VK05 tubes). Methanol (MeOH) containing internal standard was added to cecal, liver, gallbladder, portal vein tissues, and human feces. Tubes were homogenized in a MagNA Lyser. 50 μL of mouse serum and gallbladder contents were added to 50 μL of MeOH containing internal standard. Cell culture media was diluted 1:1 in MeOH. MeOH-extracted samples were centrifuged, diluted 1:1 in 50% MeOH/water, and injected into the UPLC-MS.

UPLC-MS analysis.: BA profiling by UPLC-MS was performed using a published method[43]. Total BAs in each sample were calculated by adding all detected and measured BAs. The limits of detection for individual BAs were determined using commercially available standards solubilized in 1:1 MeOH/water and are as follows: CA7S, 0.05picomol/μL; TγMCA, 0.01picomol/μL; TDCA, 0.01picomol/μL; LCA, 0.03picomol/μL; isoLCA, 0.07picomol/μL; 3-oxo-LCA, 0.05picomol/μL; DCA, 0.04picomol/μL; 3-oxo-CA, 0.04picomol/μL; 3-oxo-CDCA, 0.4picomol/μL; 7-oxo-CDCA, 0.03picomol/μL; 7-oxo-TCDCA, 0.03picomol/μL. Limits of detection of all other BAs have been reported previously[43]. All standards were purchased from Sigma, Steraloids, or Cayman Chemicals. CA7S and cholic acid-3-sulfate can be distinguished based on retention time using this UPLC-MS method.

Purification of CA7S.: Extracted cecal contents from 11 SG mice (same shown in Fig. 1) were pooled to provide sufficient material for purification. Pooled extract was purified via MS-guided HPLC of *m/z* 487 using a Luna RP C18 semi-preparative column and water and acetonitrile with 0.1% formic acid as an additive.

NMR spectroscopy.: CA7S and purified *m/z* 487 (<1 mg) were dissolved in 250 μL DMSO-d6. Nuclear magnetic resonance (NMR) spectra were acquired on a Varian INOVA 500 MHz and are referenced internally according to residual solvent signals (DMSO to 2.50, HOD to 3.33).

Cell culture.—NCI-H716 cells and Caco-2 cells were obtained from ATCC (Manassas, VA). HEK-293T cells from ATCC were a kind gift from the Blacklow lab (BCMP, HMS). Caco-2 and HEK-293T cells were maintained in MEM with GlutaMAX and Earle's Salts (Gibco, Life Technologies, UK). NCI-H716 cells were maintained in RPMI 1640 with L-glutamine (GenClone, San Diego, CA). All cell culture media were supplemented with 10% fetal bovine serum (FBS), 100 units/ml penicillin, and 100 μg/ml streptomycin (GenClone). Cells were grown in FBS- and antibiotic-supplemented 'complete' media at 37°C in an atmosphere of 5% CO_2. Testing of CA7S for agonist or antagonist activity against panels of 19 NhRs and 169 GPCRs was performed by DiscoverX. See Supplementary Note for methods.

Caco-2 cell differentiation.—Caco-2 cells were seeded in 24-well plate transwells (0.4 μM pore size, Costar) at 200,000 cells/transwell. For apical/basolateral treatments, 200,000 Caco-2 cells were mixed with 50,000 NCI-H716 cells in 6-well plate transwells (0.4 μM pore size, Costar) to mimic the ratio of epithelial cells to enteroendocrine cells in the human

colon[44]. Media was changed on days 4, 8, 12, 16, and 18 to differentiate Caco-2 cells in vitro[45]. On day 21, fully differentiated and polarized cells were validated for epithelial integrity by FITC-dextran permeability assay prior to treatment with BAs.

In vitro BA treatments.—NCI-H716 cells were seeded in cell culture plates coated with Matrigel (Corning, NY. Cat. No. 356234) diluted in HBSS (Gibco) according to manufacturer's instructions. The cells were allowed to grow for 2 days in complete RPMI media. On the day of the treatment, cells were rinsed with low serum (0.5% FBS) RPMI 1640 without antibiotics. BAs were diluted in DMSO, (VWR International) and added to cells in the low serum media (0.5% FBS, RPMI 1640) without antibiotics. DMSO concentrations were constant throughout the treatments and used as a negative control. Differentiated Caco-2 + NCI-H716 cells were treated with BAs either apically or basolaterally in low serum media (0.5% FBS, RPMI 1640) without antibiotics. NCI-H716 cells were treated in suspension with BAs for *TGR5* expression. After 2 hour incubation, media was collected in tubes containing 0.1% TFA (Sigma) in sterile water (GenClone). Cells used for GLP-1 measurements were treated with cold cell lysis solution (1% TFA, 1N hydrochloric acid, 5% formic acid, 1% NaCl), scraped off of the Matrigel, and collected in lysing tubes. For calcium measurements, cells were collected in lysing tubes with PBS. Cells were lysed in a MagNA Lyser. Cells used for RNA extraction were treated with TRIzol (Ambion, Life Technologies, Thermo Fisher Scientific, Waltham, MA) and stored at −80 °C.

GLP-1 and Insulin measurements.—Total GLP-1 measurements were performed using the GLP-1 EIA Kit (Sigma, Cat# RAB0201) and total insulin levels were measured using the Mouse Ins1/Insulin-1 ELISA kit (Sigma, Cat# RAB0817). Mouse serum samples, NCI-H716 cell lysates, and cells were stored at −80 °C and thawed on ice prior to performing assays. 20 μL of mouse serum samples were used directly in the GLP-1 ELISA assay, while 50μL of mouse serum samples were used directly in the Insulin ELISA assay. Cell culture supernatant was directly used in the GLP-1 ELISA assay. Cell lysates were subjected to peptide purification using Sep Pak C18 Classic columns (Waters Corporation, Milford, MA). The column was pretreated with a solution of 0.1% TFA in 80% isopropyl alcohol (EMD Millipore) and equilibrated with 0.1% TFA in water. Cell lysates were loaded onto the column and washed with 0.1% TFA in 80% isopropyl alcohol. The peptides were eluted in 0.1% TFA in water. The eluate was dried under vacuum and resuspended in 0.1% TFA in water. Total secreted (in media) and intracellular (cell lysates) GLP-1 were calculated using the provided standard curve. Percentage GLP-1 secretion was calculated as follows:

%GLP-1 secretion = total GLP-1 secreted (media)/(total GLP-1 secreted (media) + total GLP-1 in cell lysates)*100. Relative GLP-1 secretion was calculated compared to DMSO control.

Plasmids and transient transfections.—Human *TGR5* was cloned using cDNA from human Caco-2 cells as template, a forward primer with an *EcoRI* restriction-site (5'-CGGAATTCGCACTTGGTCCTTGTGCTCT-3'), and a reverse primer with a *XhoI*-site (5'-GTCTCGAGTTAGTTCAAGTCCAGGTCGA-3'). The PCR product was cloned into the pCDNA3.1+ plasmid (Promega Corporation, Madison, WI) and transfected at a concentration of 0.4μg/ml of media. Endogenous FXR activation was assayed using a

SHP:Luciferase reporter plasmid kindly gifted by Kristina Schoonjans (Ecole polytechnique fédérale de Lausanne-EPFL), Switzerland. For luciferase reporter assays for TGR5 activation, the cAMP response element (CRE)-driven luciferase construct pGL4.29[luc2P/CRE/Hygro] plasmid (Promega Corporation), and the pGL4.74[hRluc/CMV] plasmid (Promega Corporation) were used at concentration of 2μg/ml and 0.05μg/ml of media, respectively. For FXR activation, the SHP:Luciferase plasmid and the pGL4.74[hRluc/CMV] plasmid (Promega Corporation) were used at concentration of 2μg/ml and 0.05μg/ml of media respectively. All plasmids were transfected using Opti-MEM (Gibco) and Lipofectamine 2000 (Invitrogen, Life Technologies, Grand Island, NY, USA). Transfections were performed in appropriate antibiotic-free media with 10% FBS. After overnight incubation, BAs were added in complete media, incubated overnight, and harvested the next day for luciferase assay. *TGR5* siRNA (Santa Cruz Biotechnology, Dallas, TX) and negative siRNA (Ambion) transfection was performed using Opti-MEM and Lipofectamine. siRNAs were diluted in RNAse-free water (Genesee) and added at a final concentration of 40nM. After siRNA transfection, cells were incubated in antibiotic- and serum-free media for 24 hours and complete media for an additional 24 hours. BAs were then added (48 hours post-siRNA transfection) in complete media. After an overnight incubation, Cells were harvested for luciferase assay or RNA extraction.

Luciferase reporter assay.—Luminescence was measured using the Dual-Luciferase Reporter Assay System (Promega Corporation) according to manufacturer's instructions. Cells were washed with PBS and lysed in PLB from the kit. Matrigel-attached cells were scraped in PLB. Luminescence was measured using the SpectraMax M5 plate reader (Molecular Devices, San Jose, CA) at the ICCB-Longwood Screening Facility at HMS. Luminescence was normalized to *Renilla* luciferase activity.

Calcium measurement.—CA7S-treated NCI-H716 cells collected in PBS were used to measure intracellular calcium using the Calcium Assay Kit (Fluorometric) (Abcam, UK). Cell lysate supernatants were directly used in the calcium assay according to manufacturer's instructions. Fluorescence was measured using the SpectraMax M5 plate reader (Molecular Devices, San Jose, CA) at the ICCB-Longwood Screening Facility at HMS.

Differentiated Caco-2 permeability assay.—CA7S was added in PBS at indicated concentrations to the apical chamber of the transwells containing differentiated Caco-2 cells and incubated for 12 hours. Caco-2 epithelial integrity was assayed by measuring passive diffusion of 4 kDa FITC-Dextran (Sigma Aldrich) added at a concentration of 5 μM to the apical chamber into the basolateral chamber. Fluorescence was read on the basolateral side of the transwell system using a SpectraMax M5 plate reader (Molecular Devices, San Jose, CA) at the ICCB-Longwood Screening Facility at HMS.

Cell viability assay.—Caco-2 cells were treated with CA7S diluted in DMSO in complete MEM media. DMSO concentration was kept constant and used as a negative control. Cells were incubated with CA7S overnight at 37°C in a 5% CO_2 atmosphere. They were then treated with 0.25% trypsin in HBSS (GenClone) for 10 min at 37°C. Cell viability was measured in Countess II automated cell counter (Invitrogen).

pH stability test.—Stability of CA7S in physiological pH's was determined using the Waters pH stability test. Buffers of pH 1 (0.1M HCl), pH 7.4 (PBS) and pH 9 (10 mM ammonium formate solution adjusted to pH 9 with ammonium hydroxide) (all from Sigma) were prepared. CA7S was incubated in the pH buffers overnight at 37°C with gentle shaking (50 rpm). CA7S solution was then diluted in MeOH and injected into the UPLC-MS.

RNA extraction and qPCR.—Cells frozen in TRIzol (Ambion) were collected in Rnase-free Eppendorf tubes and vortexed. Tissues were collected in tubes with TRIzol, followed by homogenization in a MagNA Lyser (Roche, Switzerland). Differentiated cells in transwells were scraped and collected in tubes. Tubes were kept on ice whenever possible. Total RNA was extracted by chloroform-partitioning of RNA into the aqueous supernatant, followed by 2-propanol precipitating and 70% EtOH washing of the RNA pellet. The RNA pellet was air-dried and resuspended in RNase-free H_2O (GenClone). cDNA synthesis was performed using the High Capacity cDNA Reverse Transcription Kit (Applied Biosystems, Invitrogen, Foster City, CA). qPCR was performed using the Lightcycler 480 SYBR Green I Mater (Roche, Switzerland) in a 384-well format using the LightCycler 480 System (Roche), or the QuantStudio 7 (ThermoFisher) at the ICCB-Longwood Screening Facility at HMS. Cq values above 45 were considered as not detected (n.d.). The $2^{-\Delta\Delta Ct}$ method was used to calculate the relative gene expression change. Human *TGR5* gene expression were normalized to the human *HPRT1* (*HGPRT*). Mouse *Glp1r* and *Tgr5* gene expression was normalized to 18S. Primer sequences were:

human *TGR5*: Forward: 5'-CCTAGGAAGTGCCAGTGCAG-3', Reverse: 5'-CTTGGGTGGTAGGCAATGCT-3'; human *HGPRT*: Forward: 5'-CCTGGCGTCGTGATTAGTGA-3', Reverse: 5' CGAGCAAGACGTTCAGTCCT-3'; mouse *Glp1r*: Forward: 5'-AGGGCTTGATGGTGGCTATC −3', Reverse: 5'-GGACACTTGAGGGGCTTCAT −3'; mouse *Tgr5*: Forward: 5'-TTCTCTCTGTCCGCGTGTTG −3', Reverse: 5'-GGTGCTGCCCAATGAGATGA −3'; mouse *18S*: Forward: 5'ATTGGAGCTGGAATTACCGC-3', Reverse: 5'CGGCTACCACATCCAAGGAA-3'.

In vivo enteral treatment with CA7S.—13-week-old male DIO mice were purchased and housed as described in "Animals" above. Mice were weight-matched into two groups (p=0.88). After an overnight fast (17:00 to 07:00), mice received either CA7S or PBS via direct duodenal and rectal administration. The optimal, physiologic dose of CA7S was extrapolated from the average pmol concentration of CA7S in cecal samples from SG animals (average of 3000pmol/mg of stool with 500mg of stool per animal corresponds to 0.75mg of CA7S per cecum).

Under isoflurane general anesthesia, 0.25 mg and 0.75 mg of CA7S in PBS (pH 7.2) was delivered by slow infusion (5 min) antegrade into the duodenum and retrograde into the rectum, respectively. The total volume of instillation was 2 mL (0.5 mg CA7S/mL). Control animals received similar volumes of PBS alone. 15 min post infusion, serum glucose was measured via tail vein followed by whole blood collection via cardiac puncture into K +EDTA tubes containing DPPIV inhibitor (Merck Millipore, Billerica, MA), Perfabloc (Sigma), and apoprotinin (Sigma). One glucose reading from the PBS group was occluded

by a clot, therefore was excluded from glucose analysis. Whole blood and tissues were harvested for analysis. In order to account for changes in fasting times and hormonal diurnal rhythms, this experiment was carried out on four consecutive days such that only four mice were tested per day.

In vivo acute CA7S gavage.—16-week-old DIO mice were purchased and housed as described in “Animals” above. Mice were fasted for 4 hours on the day of the experiment. Mice were orally gavaged with 100 mg/kg CA7S from 20 mg/mL solution, or equivalent volume of PBS. 5 hours after administration, whole blood and tissues were collected in the fasted state. One liver sample from the CA7S group was lost during sample preparation, therefore was excluded from BA analysis.

In vivo CA7S and OGTT.—16-week-old DIO mice were purchased and housed as described in “Animals” above. Blood glucose levels were monitored until average fasting glucose levels were >160 mg/dL. Animals were fasted for 4 hours on the day of the experiment. Mice were matched into two groups based on fasting glucose levels and received either 100 mg/kg CA7S from a 20 mg/ml solution or an equivalent volume of PBS by oral gavage. Three hours later, an OGTT was performed using an oral gavage of 2 mg/g oral D-glucose (Sigma-Aldrich, St. Louis, MO). Serum glucose was measured at baseline and at minutes 15, 30, 60 and 120 with a OneTouch glucometer.

Lentiviral IP injection.—*Glp1r* and *Tgr5* shRNA-containing lentiviral particles (LVP) were purchased from the MISSION TRC library (Sigma-Aldrich, St. Louis, MO). LVPs containing a mixture of three *Glp1r* shRNA plasmid clones (TRCN0000004629, TRCN0000004630, and TRCN0000004633) and *Tgr5* shRNA plasmid clones (TRCN0000026777, TRCN0000026783, TRCN0000026817) were purchased. Mice were maintained on a HFD until average fasting glucose >160 mg/dL in a BL2 facility. Under sterile conditions, mice were injected intraperitoneally with 0.2 mL of 5×10^5 shRNA LVPs[46,47]. 72 hours after injection, mice underwent CA7S/PBS gavage followed by OGTT as above. After the OGTT was completed, mice were sacrificed and their tissues were harvested. *Glp1r* and *Tgr5* knockdown efficiency was measured in tissues by qPCR as described above.

CA7S chronic feeding.—16-week-old DIO mice were purchased and housed as described above in “Animals”. Mice were orally gavaged daily for 48 days with 100 mg/kg CA7S or equivalent volume of PBS. Weight and food intake were measured daily. Both groups of mice exhibited initial weight loss during the experiment, presumably due to the stress of daily gavage. Mice were fasted overnight prior to sacrifice. Fasting glucose was measured at sacrifice. Whole blood and tissues were collected. Two gallbladders in the CA7S group perforated prior to weighing and therefore were excluded from analysis. One liver sample from the CA7S group was lost following harvest and thus not included in the analysis.

Human stool collection.—After obtaining institutional review board approval and informed consent, we prospectively collected stool specimen from obese human subjects undergoing SG. Patents were selected randomly over the course of a one-year enrollment

with the following exclusion criteria: 1) antibiotic use within 3 months of surgery, 2) on immunosuppressants, 3) pre-existing immunocompromised state, 4) chronic diarrhea, 5) Ulcerative colitis or Crohn's disease, 6) prior colon resection. For each patient, a pre-operative stool specimen collected on the day of surgery was compared to a stool specimen obtained from post-operative day 14 to 99 (mode 15 days; median 36 days). Specimens were snap frozen in liquid nitrogen and stored at −80 ºC until BA analysis was performed by a blinded investigator.

Ethics.—All mouse experiments were performed under the approval of the Brigham and Women's Hospital IACUC. Human stool collection was performed under the approval of the Brigham and Women's Hospital IRB.

Statistics and Reproducibility

No statistical methods were used to predetermine sample size. Sample sizes were determined by magnitude and consistency of measurable differences. Statistical tests used for each experiment are outlined in the figure legends. All data are presented as mean ± SEM. All in vitro studies represented in the publication were performed in at least 3 biological replicates. Each experiment was reproduced in triplicate at least twice with similar results. In vivo mouse studies: The sleeve gastrectomy model is well established in the Sheu lab. The functional glucose data (IPGTT and ITT) is in keeping with previously published data from other labs. [6,48] Thus, the number of mice used was kept to a minimum and replicate testing was not performed for the Sham and SG surgeries. Bile acid were analyzed from four independently performed Sham and SG surgeries over the course of a year, and the data in the manuscript represents all the replicates. CA7S enteral administration was not replicated owing to the clear significance of the results. CA7S acute gavage was performed in two independent experiments with similar results. The lentiviral knockdown experiments were performed in two independent experiments with similar results. The chronic dosing experiment (Fig. 6) results were reproduced in an independent cohort of mice (n=7) dosed with higher concentrations of CA7S. The paper includes 3 mouse studies (Figs. 4, 5, 6) which were performed by 3 different investigators (D.A.H., H.A., J.L. respectively) at different times, thereby providing reproducible corroboration that CA7S remains gut-restricted and improves hyperglycemia. Human stool samples from bariatric surgery patients were a scarce resource. We used all available samples and as such did not have samples available for replicate experiments. P values of less than 0.05 were considered significant. Unless stated otherwise, the experiments were not randomized, and investigators were not blinded to allocation during in vitro and in vivo experiments.

Software

GraphPad Prism (version 8) software was used to plot data and perform statistical analyses. ChemDraw software (version 12) was used to draw chemical structures.

Data availability statement

All data generated or analyzed during this study are included in this article and its supplementary information and extended data files.

Code availability statement

No custom code or mathematical algorithms were used in this study.

Extended Data

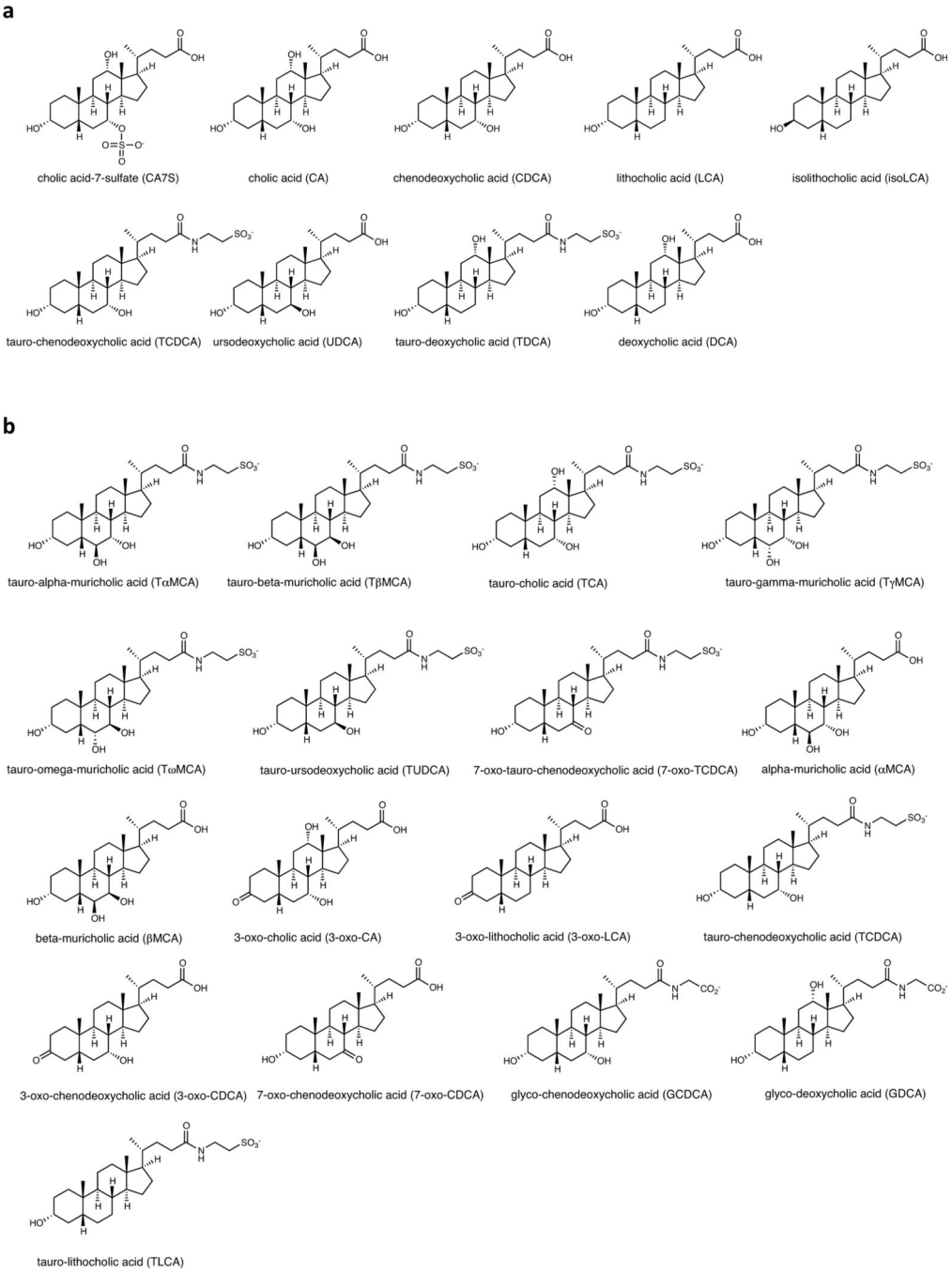

Extended Data Fig. 1. Bile acid structures

a, Structures of bile acids in main text and figures. **b**, Structures of additional bile acids in Extended Data and Supplementary Information.

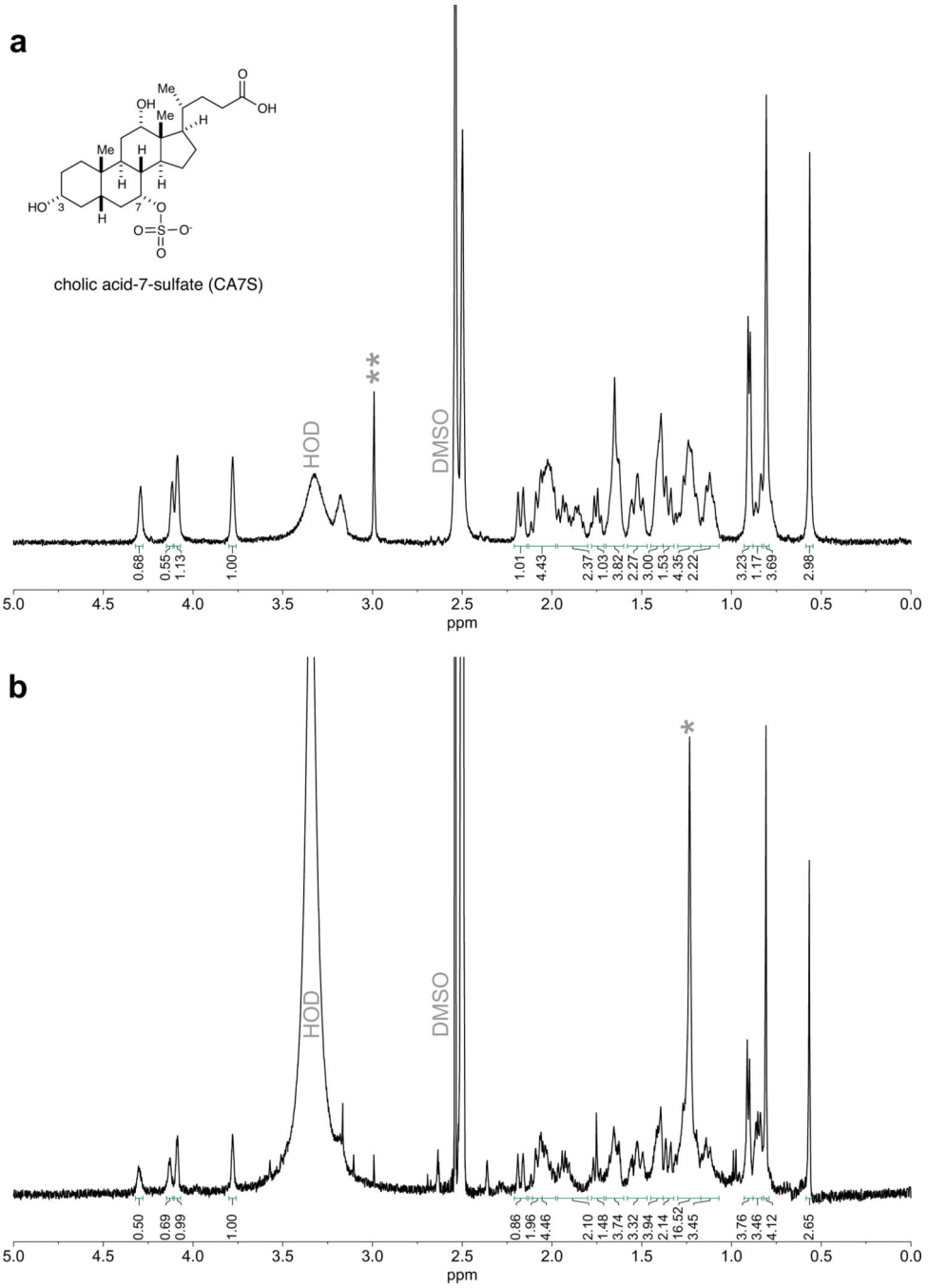

Extended Data Fig. 2. NMR of cholic acid-7-sulfate

a, ^{1}H NMR of authentic sample of cholic acid-7-sulfate (CA7S) (Cayman Chemical). **b**, ^{1}H NMR of CA7S purified from the cecal contents of SG mice. Signals between 3.7 to 4.4 ppm are diagnostic of CA7S. Impurities are denoted by asterisks.

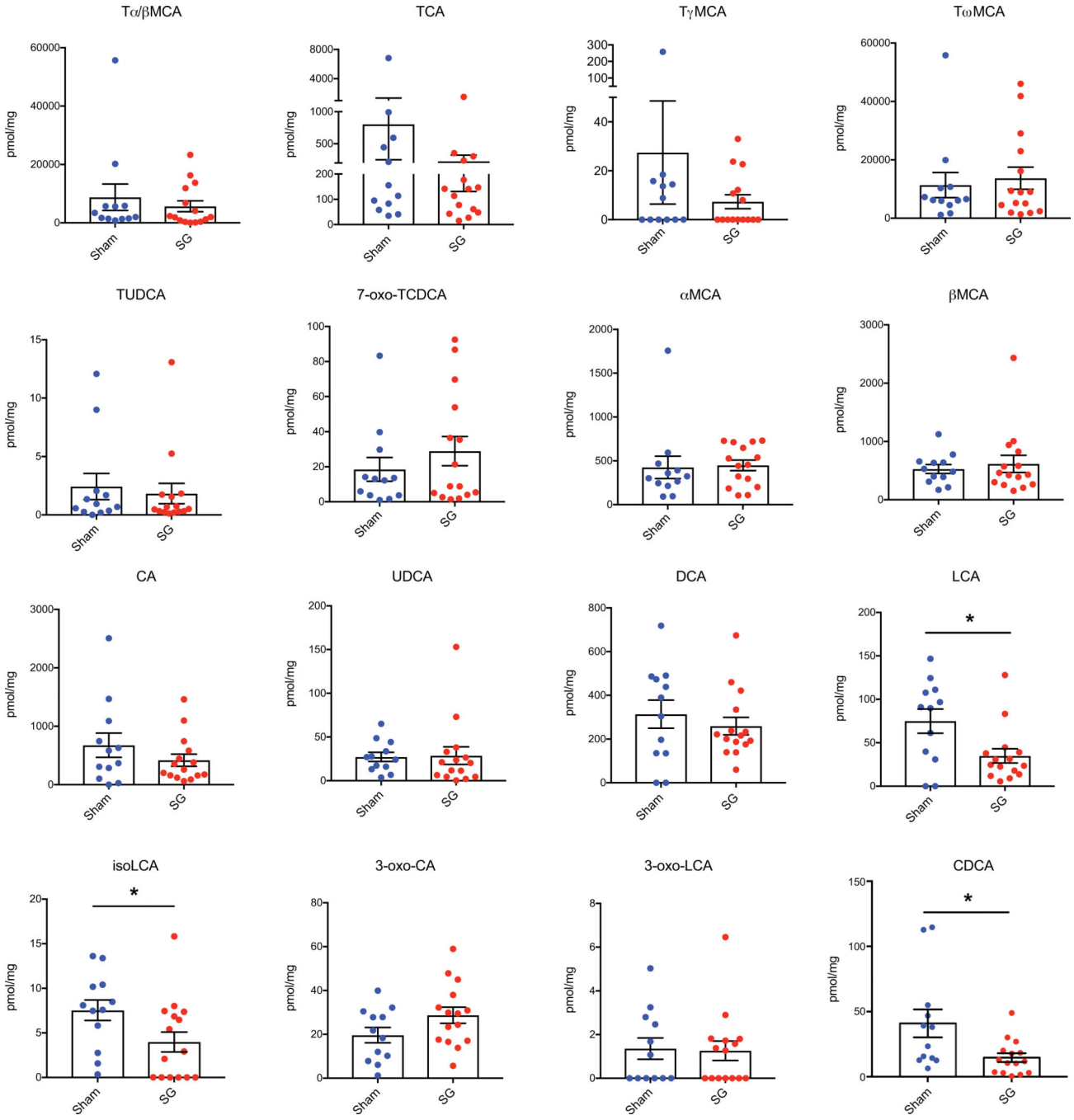

Extended Data Fig. 3. Bile acid concentrations in cecal contents of mice post-sham or post-SG

Six weeks following surgery, cecal contents were collected from sham or SG mice after an overnight fast. Bile acids were quantified using UPLC-MS (sham, n=12, SG, n=15, data not marked with asterisk(s) are not significant). All bile acids with measurable concentrations above the limit of detection are shown. Tα/βMCA, tauro-alpha- and tauro-beta-muricholic acid, p=0.53; TCA, tauro-cholic acid, p=0.32; TγMCA, tauro-gamma-muricholic acid, p=0.36; TωMCA, tauro-omega-muricholic acid, p=0.68; TUDCA, tauro-ursodeoxycholic acid, p=0.67; 7-oxo-TCDCA, 7-oxo-tauro-chenodeoxycholic acid p=0.34; αMCA, alpha-

muricholic acid, p=0.87; βMCA, beta-muricholic acid, p=0.59; CA, cholic acid, p=0.28; UDCA, ursodeoxycholic acid, p=0.85; DCA, deoxycholic acid, p=0.48; LCA, lithocholic acid, *p=0.02; isoLCA, isolithocholic acid *p=0.02; 3-oxo-CA, 3-oxo-cholic acid, p=0.08; 3-oxo-LCA, 3-oxo-lithocholic acid, p=0.79; CDCA, chenodeoxycholic acid, *p=0.03, two-tailed Welch's t-test. All data are presented as mean ± SEM.

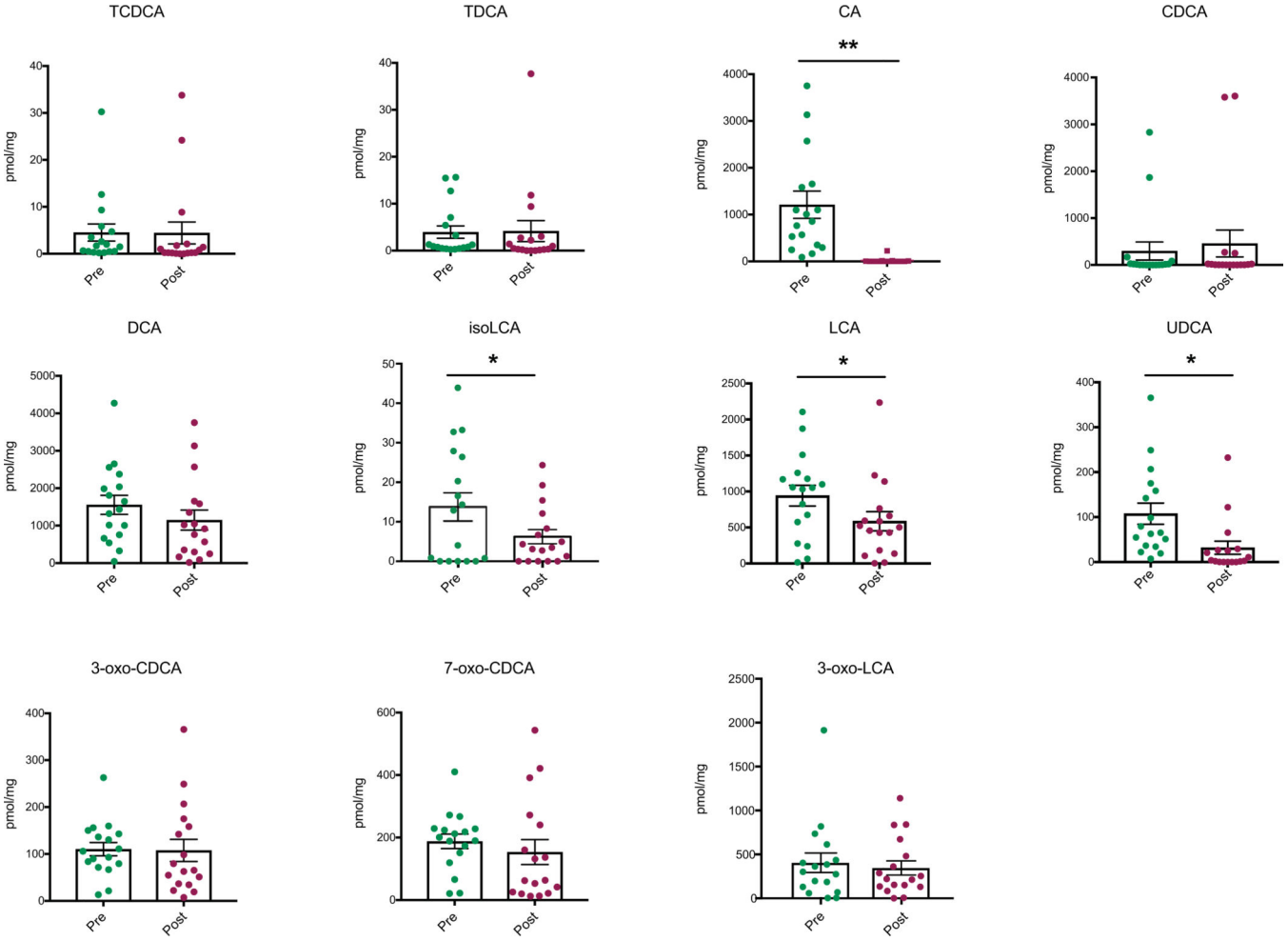

Extended Data Fig. 4. Bile acid concentrations in feces of human patients pre-SG or post-SG

Feces were collected from patients pre-op or ~5 weeks post-op and bile acids were quantified using UPLC-MS (n=17 patients, median 36 days after surgery, data not marked with asterisk(s) are not significant). All bile acids with measurable concentrations above the limit of detection are shown. TCDCA, tauro-chenodeoxycholic acid, p=0.97; TDCA, tauro-deoxycholic acid, p=0.93; CA, cholic acid, **p=1.00×10^{-3}; CDCA, chenodeoxycholic acid, p=0.52; DCA, deoxycholic acid, p=0.13; LCA, lithocholic acid, *p=0.01; isoLCA, iso-lithocholic acid, *p=0.03; UDCA, ursodeoxycholic acid, *p=0.02; 3-oxo-CDCA, 3-oxo-chenodeoxycholic acid, p=0.92; 7-oxo-CDCA, 7-oxo-chenodeoxycholic acid, p=0.47, 3-oxo-LCA, 3-oxo-lithocholic acid, p=0.56, two-tailed paired t-test. All data are presented as mean ± SEM.

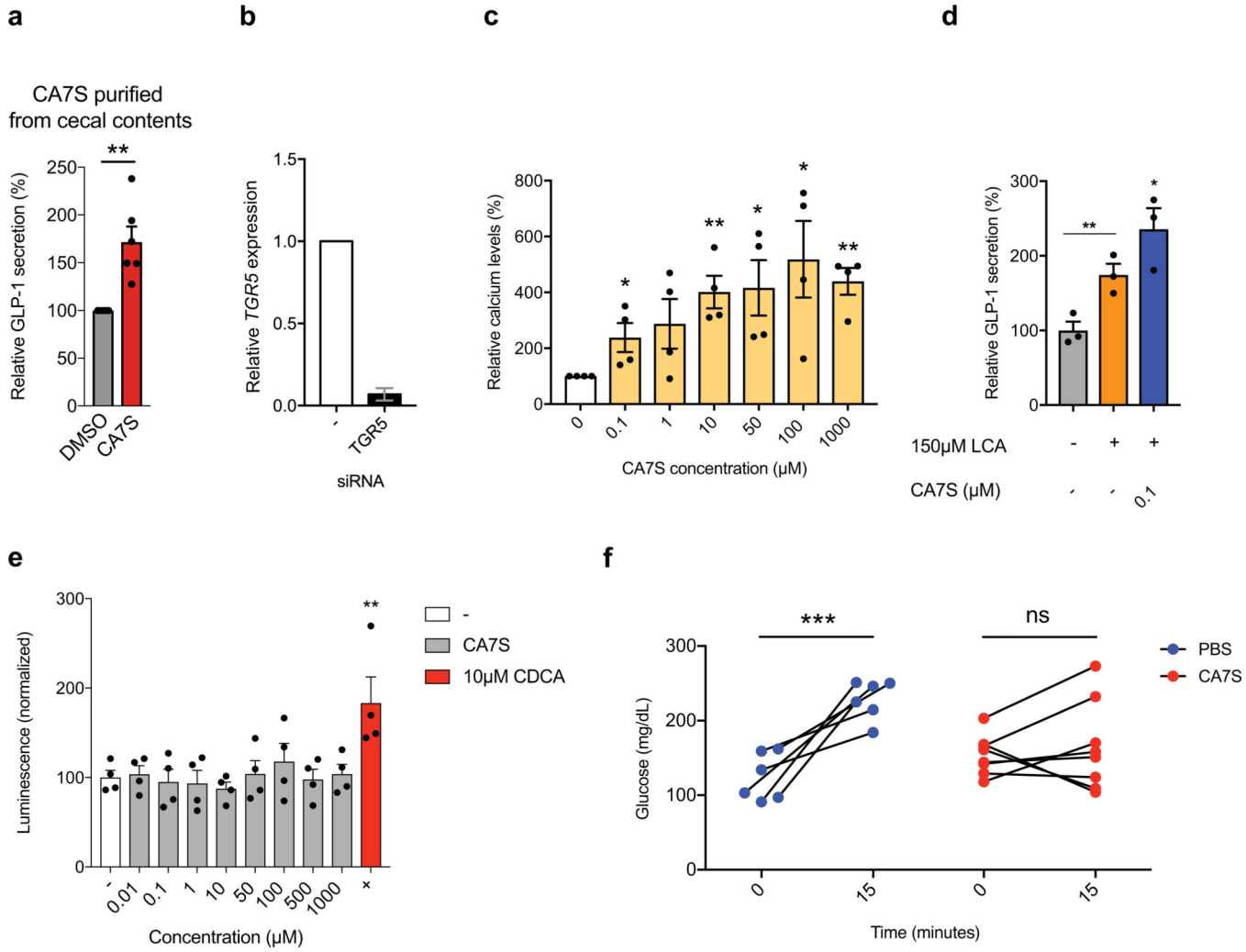

Extended Data Fig. 5. CA7S agonizes TGR5 but not FXR, induces GLP-1 secretion, and reduces systemic glucose levels

a, CA7S (500 μM) purified from SG mouse cecal contents induced secretion of GLP-1 in NCI-H716 cells compared to DMSO control (6 biological replicates per condition, $^{**}p=1.00\times10^{-3}$, two-tailed Welch's t-test). **b**, Quantitative real time PCR analysis of expression of human *TGR5* in *TGR5* siRNA and negative (−) siRNA-treated NCI-H716 cells for Fig. 3b. **c**, CA7S induced an increase in intracellular calcium levels in NCI-H716 cells (4 biological replicates per condition, CA7S 10 μM $^{*}p=0.03$, 50 μM $^{*}p=0.02$, 100 μM $^{**}p=1.80\times10^{-3}$, 100 μM $^{*}p=0.01$, one-way ANOVA followed by Dunnett's multiple comparisons test). **d**, CA7S induced secretion of GLP-1 in the presence of a physiologically relevant concentration of LCA (150 μM) (3 biological replicates per condition, DMSO (−) control vs. LCA $^{**}p=9.90\times10^{-3}$, CA7S vs. LCA 0.1 μM $^{*}p=0.03$, two-way ANOVA followed by Dunnett's multiple comparisons test). **e**, CA7S did not induce activation of endogenous FXR in Caco-2 cells compared to (−) DMSO control. Known FXR agonist CDCA (10 μM) was used as a positive control (4 biological replicates per condition, CA7S 0.01–50 μM and 500–1000 μM not significant $p=0.99$, CA7S 100 μM not significant $p=0.96$, CDCA 10 μM $^{**}p=4.60\times10^{-3}$, one-way ANOVA followed by Dunnett's multiple

comparisons test). **f**, In vivo change in serum glucose upon acute enteral treatment with PBS and CA7S (PBS, n=6; CA7S, n=8 mice, ***p=1.00×10^{-4}, ns=not significant p=0.63, two-tailed paired t-test). All data are presented as mean ± SEM.

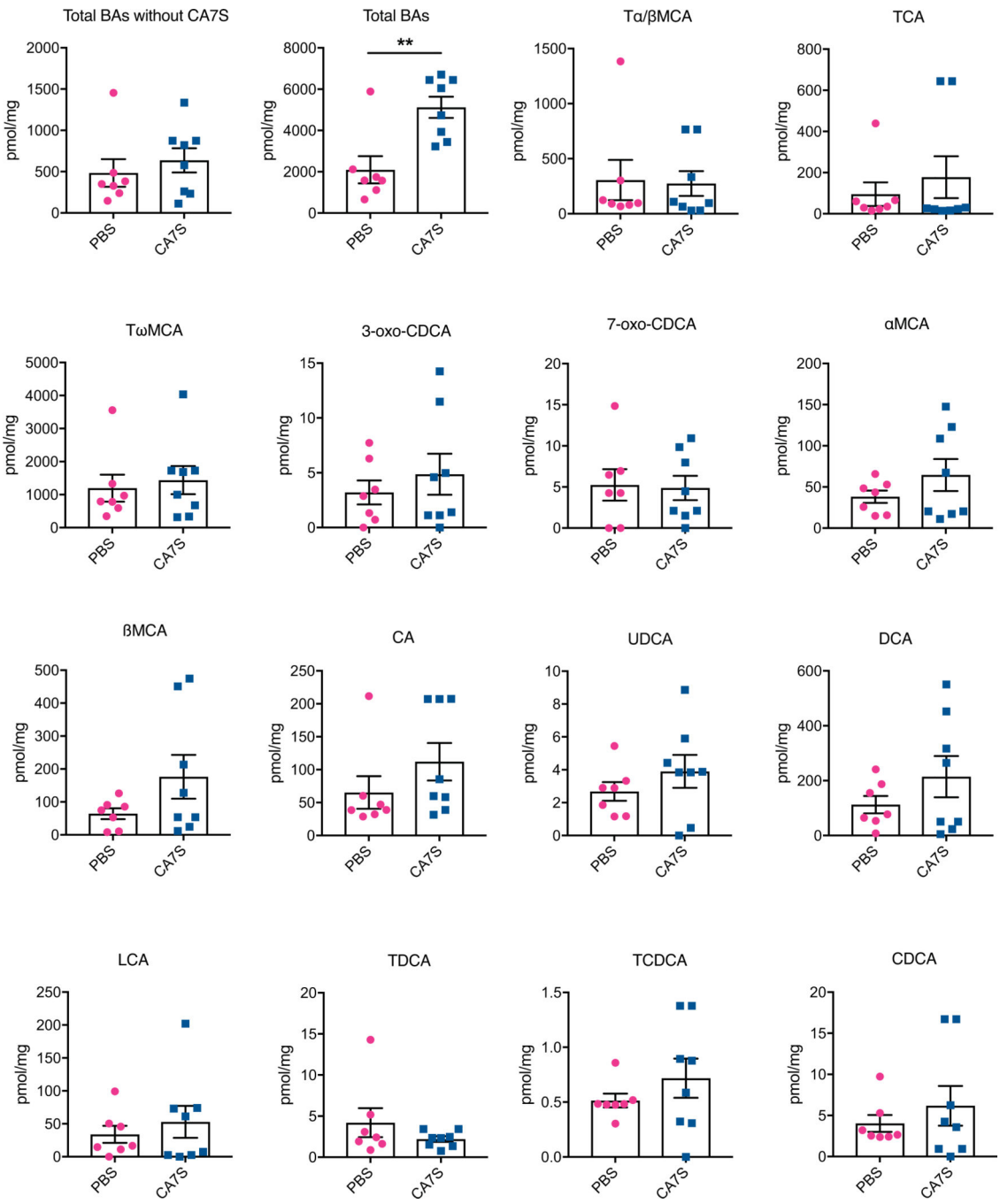

Extended Data Fig. 6. Bile acid concentrations in cecal contents of mice treated enterally with CA7S

Cecal contents were collected from mice after enteral treatment with CA7S or PBS and bile acids were quantified using UPLC-MS (PBS, n=7, CA7S, n=8, data not marked with asterisk(s) are not significant). All bile acids with measurable concentrations above the limit

of detection are shown. Total BAs without CA7S, p=0.50; Total bile acids (BAs), **p=3.5×10^{-3}; Tα/βMCA, tauro-alpha- and tauro-beta-muricholic acid, p=0.88; TCA, tauro-cholic acid, p=0.49; TωMCA, tauro-omega-muricholic acid, p=0.68; 3-oxo-CDCA, 3-oxo-chenodeoxycholic acid p=0.45; 7-oxo-CDCA, 7-oxo-chenodeoxycholic acid p=0.87; αMCA, alpha-muricholic acid, p=0.23; βMCA, beta-muricholic acid, p=0.14; CA, cholic acid, p=0.23; UDCA, ursodeoxycholic acid, p=0.30; DCA, deoxycholic acid, p=0.24; LCA, lithocholic acid, p=0.50; TDCA, tauro-deoxycholic acid, p=0.30; TCDCA, tauro-chenodeoxycholic acid, p=0.31; CDCA, chenodeoxycholic acid, p=0.43, two-tailed Welch's t-test. All data are presented as mean ± SEM.

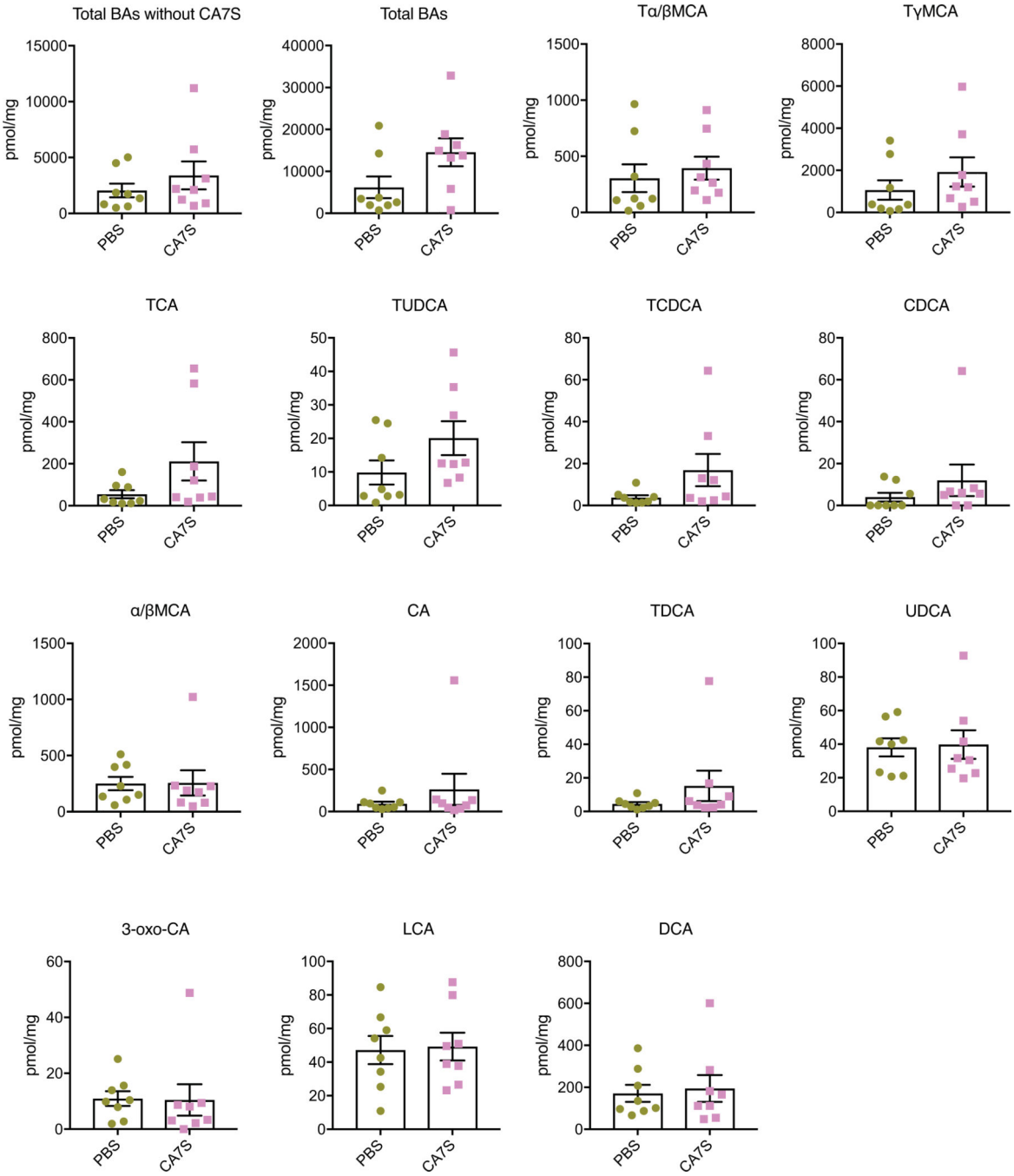

Extended Data Fig. 7. Bile acid concentrations in cecal contents of mice gavaged with one dose of CA7S

Fasted DIO mice were gavaged with CA7S or PBS and cecal contents were collected from mice 5 hours post-gavage. Bile acids were quantified using UPLC-MS (n=8 in each group, data not marked with asterisk(s) are not significant). All bile acids with measurable concentrations above the limit of detection are shown. Total BAs without CA7S, p=0.35; Total bile acids (BAs), p=0.06; Tα/βMCA, tauro-alpha- and tauro-beta-muricholic acid, p=0.58; TγMCA, tauro-gamma-muricholic acid, p=0.32; TCA, tauro-cholic acid, p=0.13; TUDCA, tauro-ursodeoxycholic acid, p=0.12; TCDCA, tauro-chenodeoxycholic acid,

p=0.13; CDCA, chenodeoxycholic acid, *p*=0.33; αβMCA, alpha-muricholic acid and beta-muricholic acid, *p*=0.96; CA, cholic acid, *p*=0.38; TDCA, tauro-deoxycholic acid, *p*=0.27; UDCA, ursodeoxycholic acid, *p*=0.87; 3-oxo-CA, 3-oxo-cholic acid, *p*=0.93; LCA, lithocholic acid, *p*=0.86; DCA, deoxycholic acid, *p*=0.76, two-tailed Welch's t-test. All data are presented as mean ± SEM.

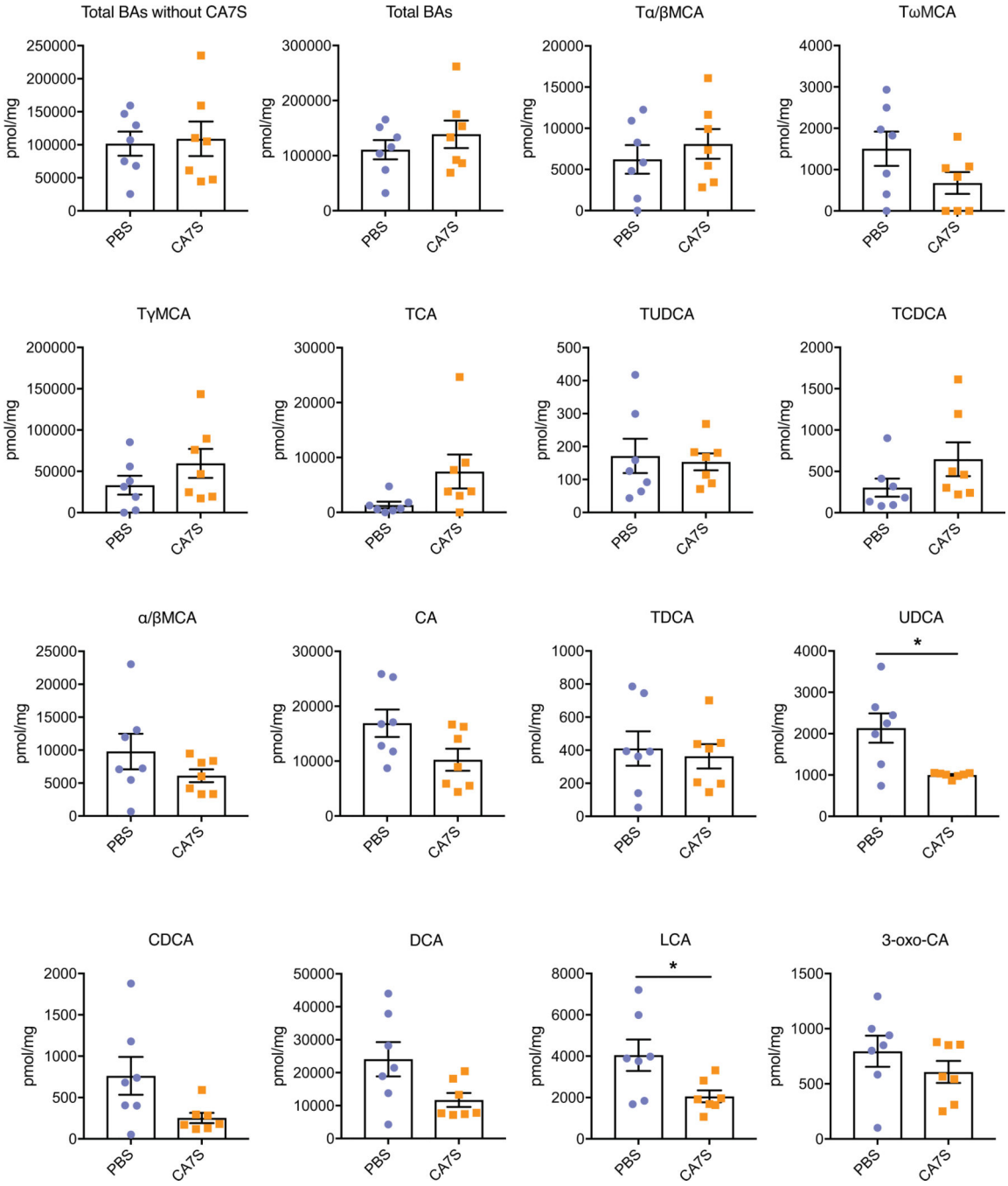

Extended Data Fig. 8. Bile acid concentrations in cecal contents of mice gavaged chronically with CA7S

Cecal contents were collected from mice following an overnight fast after 48 days of daily gavage with CA7S or PBS. Bile acids were quantified using UPLC-MS (n=7 in each group, data not marked with asterisk(s) are not significant). All bile acids with measurable concentrations above the limit of detection are shown. Total BAs without CA7S, p=0.82; Total bile acids (BAs), p=0.38; Tα/βMCA, tauro-alpha- and tauro-beta-muricholic acid, p=0.46; TωMCA, tauro-omega-muricholic acid, p=0.12; TγMCA, tauro-gamma-muricholic acid, p=0.23; TCA, tauro-cholic acid, p=0.09; TUDCA, tauro-ursodeoxycholic acid, p=0.76; TCDCA, tauro-chenodeoxycholic acid, p=0.17; αβMCA, alpha-muricholic acid and beta-muricholic acid, p=0.23; CA, cholic acid, p=0.06; TDCA, tauro-deoxycholic acid, p=0.71; UDCA, ursodeoxycholic acid, *p=0.01; CDCA, chenodeoxycholic acid, p=0.06; DCA, deoxycholic acid, p=0.23; LCA, lithocholic acid, *p=0.04; 3-oxo-CA, 3-oxo-cholic acid, p=0.30, two-tailed Welch's t-test. All data are presented as mean ± SEM.

Supplementary Material

Refer to Web version on PubMed Central for supplementary material.

Acknowledgements

We thank members of the Devlin, Sheu, Clardy, and Banks labs (Harvard Medical School-HMS) for helpful discussions and advice. We would like to acknowledge the Blacklow and Kruse labs for help with equipment and reagents, and the BWH mouse facility. We would like to thank K. Schoonjans (Ecole polytechnique fédérale de Lausanne-EPFL) for the FXR reporter plasmid. We are grateful to the human patients who participated in this study. This work was supported by a KL2 award from Harvard Catalyst (4Kl2TR001100-04) (E.G.S.), a pilot grant from Boston Area Diabetes and Endocrinology Research Center (BADERC) (NIH/NIDDK P30 DK057521) (E.G.S.), an NIH MIRA grant (R35 GM128618) (A.S.D.), a Blavatnik Biomedical Accelerator at Harvard University grant (A.S.D.), a Quadrangle Fund for the Advancement and Seeding of Translational Research at Harvard Medical School (Q-FASTR) grant (A.S.D. and E.G.S.), an American Heart Association Postdoctoral Fellowship (S.N.C.), a HMS Department of Biological Chemistry and Molecular Pharmacology Fellowship (S.N.C), an American College of Surgeons fellowship (D.A.H.), an NIH T32 training grant (D.A.H. and J.N.L), and a DRC P&F program grant from the Joslin Diabetes Center (P30DK036836) (A.H.V).

References

1. Batterham RL & Cummings DE Mechanisms of Diabetes Improvement Following Bariatric/Metabolic Surgery. Diabetes Care 39, 893–901 (2016). [PubMed: 27222547]
2. Gloy VL et al. Bariatric surgery versus non-surgical treatment for obesity: a systematic review and meta-analysis of randomised controlled trials. BMJ 347, f5934–f5934 (2013).
3. Abbasi J. Unveiling the 'Magic' of Diabetes Remission After Weight-Loss Surgery. JAMA 317, 571–574 (2017). [PubMed: 28196253]
4. Kaska L, Sledzinski T, Chomiczewska A, Dettlaff-Pokora A. & Swierczynski J. Improved glucose metabolism following bariatric surgery is associated with increased circulating bile acid concentrations and remodeling of the gut microbiome. World J. Gastroenterol 22, 8698–8719 (2016). [PubMed: 27818587]
5. Fiorucci S. & Distrutti E. Bile Acid-Activated Receptors, Intestinal Microbiota, and the Treatment of Metabolic Disorders. Trends Mol Med 21, 702–714 (2015). [PubMed: 26481828]
6. Ryan KK et al. FXR is a molecular target for the effects of vertical sleeve gastrectomy. Nature 509, 183–188 (2014). [PubMed: 24670636]
7. Patti M-E et al. Serum bile acids are higher in humans with prior gastric bypass: potential contribution to improved glucose and lipid metabolism. Obesity (Silver Spring) 17, 1671–1677 (2009). [PubMed: 19360006]

8. Sayin SI et al. Gut microbiota regulates bile acid metabolism by reducing the levels of tauro-beta-muricholic acid, a naturally occurring FXR antagonist. Cell Metab. 17, 225–235 (2013). [PubMed: 23395169]

9. Duboc H, Taché Y. & Hofmann AF The bile acid TGR5 membrane receptor: from basic research to clinical application. Dig Liver Dis 46, 302–312 (2014). [PubMed: 24411485]

10. Madsbad S. The role of glucagon-like peptide-1 impairment in obesity and potential therapeutic implications. Diabetes Obes Metab 16, 9–21 (2014). [PubMed: 23617798]

11. Khorgami Z. et al. Trends in utilization of bariatric surgery, 2010–2014: sleeve gastrectomy dominates. Surg Obes Relat Dis 13, 774–778 (2017). [PubMed: 28256393]

12. Lutz TA & Bueter M. The Use of Rat and Mouse Models in Bariatric Surgery Experiments. Front Nutr 3, 25 (2016). [PubMed: 27547753]

13. Alnouti Y. Bile Acid sulfation: a pathway of bile acid elimination and detoxification. Toxicol. Sci 108, 225–246 (2009). [PubMed: 19131563]

14. Sato H. et al. Novel Potent and Selective Bile Acid Derivatives as TGR5 Agonists: Biological Screening, Structure−Activity Relationships, and Molecular Modeling Studies. Journal of Medicinal Chemistry 51, 1831–1841 (2008). [PubMed: 18307294]

15. Kawamata Y. et al. A G protein-coupled receptor responsive to bile acids. J. Biol. Chem 278, 9435–9440 (2003). [PubMed: 12524422]

16. Maruyama T. et al. Identification of membrane-type receptor for bile acids (M-BAR). Biochem. Biophys. Res. Commun 298, 714–719 (2002). [PubMed: 12419312]

17. Sato H. et al. Anti-hyperglycemic activity of a TGR5 agonist isolated from Olea europaea. Biochem. Biophys. Res. Commun 362, 793–798 (2007). [PubMed: 17825251]

18. Rizzo G. et al. Functional characterization of the semisynthetic bile acid derivative INT-767, a dual farnesoid X receptor and TGR5 agonist. Mol. Pharmacol 78, 617–630 (2010). [PubMed: 20631053]

19. Pellicciari R. et al. Discovery of 6alpha-ethyl-23(S)-methylcholic acid (S-EMCA, INT-777) as a potent and selective agonist for the TGR5 receptor, a novel target for diabesity. Journal of Medicinal Chemistry 52, 7958–7961 (2009). [PubMed: 20014870]

20. Thomas C. et al. TGR5-mediated bile acid sensing controls glucose homeostasis. Cell Metab. 10, 167–177 (2009). [PubMed: 19723493]

21. Brighton CA et al. Bile Acids Trigger GLP-1 Release Predominantly by Accessing Basolaterally Located G Protein-Coupled Bile Acid Receptors. Endocrinology 156, 3961–3970 (2015). [PubMed: 26280129]

22. Kuhre RE et al. Peptide production and secretion in GLUTag, NCI-H716, and STC-1 cells: a comparison to native L-cells. Journal of Molecular Endocrinology 56, 201–211 (2016). [PubMed: 26819328]

23. Kuhre RE et al. Bile acids are important direct and indirect regulators of the secretion of appetite- and metabolism-regulating hormones from the gut and pancreas. Mol Metab 11, 84–95 (2018). [PubMed: 29656109]

24. Guo C, Chen W-D & Wang Y-D TGR5, Not Only a Metabolic Regulator. Front Physiol 7, 646 (2016). [PubMed: 28082913]

25. Hamilton JP et al. Human cecal bile acids: concentration and spectrum. Am. J. Physiol. Gastrointest. Liver Physiol 293, G256–G263 (2007). [PubMed: 17412828]

26. Comeglio P. et al. INT-767 prevents NASH and promotes visceral fat brown adipogenesis and mitochondrial function. J. Endocrinol 238, 107–127 (2018). [PubMed: 29945982]

27. Pathak P. et al. Farnesoid X receptor induces Takeda G-protein receptor 5 cross-talk to regulate bile acid synthesis and hepatic metabolism. J. Biol. Chem 292, 11055–11069 (2017).

28. Chen M-C, Chen Y-L, Wang T-W, Hsu H-P & Lai M-D Membrane bile acid receptor TGR5 predicts good prognosis in ampullary adenocarcinoma patients with hyperbilirubinemia. Oncol. Rep 36, 1997–2008 (2016). [PubMed: 27510297]

29. Xiong Q. et al. Metabolite-Sensing G Protein Coupled Receptor TGR5 Protects Host From Viral Infection Through Amplifying Type I Interferon Responses. Front Immunol 9, 2289 (2018). [PubMed: 30333836]

30. Eissele R. et al. Glucagon-like peptide-1 cells in the gastrointestinal tract and pancreas of rat, pig and man. Eur. J. Clin. Invest 22, 283–291 (1992). [PubMed: 1499644]
31. Harach T. et al. TGR5 potentiates GLP-1 secretion in response to anionic exchange resins. Sci Rep 2, 430 (2012). [PubMed: 22666533]
32. Ferruzza S, Rossi C, Scarino ML & Sambuy Y. A protocol for differentiation of human intestinal Caco-2 cells in asymmetric serum-containing medium. Toxicol In Vitro 26, 1252–1255 (2012). [PubMed: 22265977]
33. Tan H-Y et al. A multi-chamber microfluidic intestinal barrier model using Caco-2 cells for drug transport studies. PLOS ONE 13, e0197101 (2018).
34. Wilson-Pérez HE et al. Vertical sleeve gastrectomy is effective in two genetic mouse models of glucagon-like Peptide 1 receptor deficiency. Diabetes 62, 2380–2385 (2013). [PubMed: 23434938]
35. McGavigan AK et al. TGR5 contributes to glucoregulatory improvements after vertical sleeve gastrectomy in mice. Gut 66, 226–234 (2017). [PubMed: 26511794]
36. Hodge RJ & Nunez DJ Therapeutic potential of Takeda-G-protein-receptor-5 (TGR5) agonists. Hope or hype? Diabetes Obes Metab 18, 439–443 (2016). [PubMed: 26818602]
37. Cao H. et al. Intestinally-targeted TGR5 agonists equipped with quaternary ammonium have an improved hypoglycemic effect and reduced gallbladder filling effect. Sci Rep 6, 28676 (2016).
38. Wang S. et al. Interplay between bile acids and the gut microbiota promotes intestinal carcinogenesis. Mol. Carcinog 58, 1155–1167 (2019). [PubMed: 30828892]
39. Dawson PA & Setchell KDR Will the real bile acid sulfotransferase please stand up? Identification of Sult2a8 as a major hepatic bile acid sulfonating enzyme in mice. J. Lipid Res 58, 1033–1035 (2017). [PubMed: 28455387]
40. Beuers U, Trauner M, Jansen P. & Poupon R. New paradigms in the treatment of hepatic cholestasis: from UDCA to FXR, PXR and beyond. Journal of Hepatology 62, S25–37 (2015). [PubMed: 25920087]
41. Ma K, Saha PK, Chan L. & Moore DD Farnesoid X receptor is essential for normal glucose homeostasis. Journal of Clinical Investigation 116, 1102–1109 (2006).
42. Schaap FG, Trauner M. & Jansen PLM Bile acid receptors as targets for drug development. Nat Rev Gastroenterol Hepatol 11, 55–67 (2014). [PubMed: 23982684]

Methods-only References

43. Yao L. et al. A selective gut bacterial bile salt hydrolase alters host metabolism. eLife 7, e37182 (2018).
44. Cristina ML, Lehy T, Zeitoun P. & Dufougeray F. Fine structural classification and comparative distribution of endocrine cells in normal human large intestine. Gastroenterology 75, 20–28 (1978). [PubMed: 95721]
45. Verhoeckx K. et al. Caco-2 Cell Line. The Impact of Food Bioactives on Health 175, 103–111 (2015).
46. Tiscornia G, Singer O, Ikawa M. & Verma IM A general method for gene knockdown in mice by using lentiviral vectors expressing small interfering RNA. PNAS 100, 1844–1848 (2003). [PubMed: 12552109]
47. Blosser W. et al. A method to assess target gene involvement in angiogenesis in vitro and in vivo using lentiviral vectors expressing shRNA. PLOS ONE 9, e96036 (2014).
48. Abu-Gazala S. et al. Sleeve Gastrectomy Improves Glycemia Independent of Weight Loss by Restoring Hepatic Insulin Sensitivity. Diabetes 67, 1079–1085 (2018). [PubMed: 29475831]

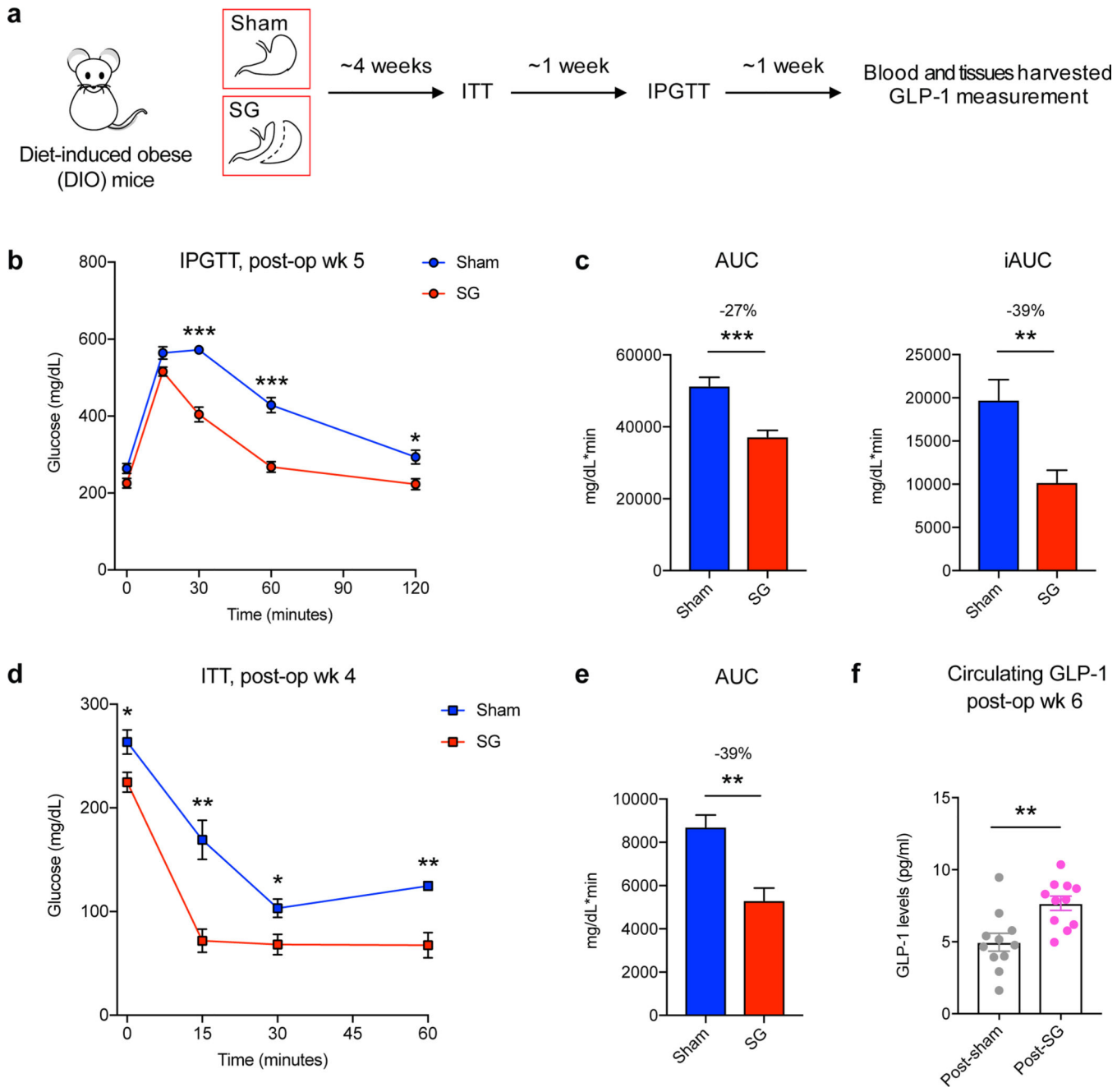

Figure 1. DIO mice display improved glucose tolerance and insulin sensitivity following SG

a, Schematic of surgical interventions and post-operative assessments. Sleeve gastrectomy (SG) or sham surgery was performed on diet-induced obese (DIO) mice, followed by an insulin tolerance test (ITT) ~4 weeks post-op and then intraperitoneal glucose tolerance test (IPGTT) ~5 weeks post-op. Blood and tissues were harvested ~6 weeks post-op in the fasted state. **b**, Glycemic curves during IPGTT (SG, n=7; sham, n=6, 30 min ***p=5.91×10^{-6}, 60 min ***p=4.34×10^{-5}, 120 min *p=0.01, two-tailed Student's t-test). **c**, Corresponding area under the blood glucose curve (AUC) and incremental area under the curve (iAUC) were reduced in SG- compared to sham-operated mice. (SG, n=7; sham, n=6, AUC ***p=

4.01×10^{-4}, iAUC $^{**}p=6.12\times10^{-3}$, two-tailed Welch's t-test). **d**, Glycemic curves during ITT (SG, n=4; sham, n=4, 0 min $^{*}p=0.04$, 15 min $^{**}p=4.31\times10^{-3}$, 30 min $^{*}p=0.03$, 60 min $^{**}p=4.53\times10^{-3}$, two-tailed Student's t-test). **e**, Corresponding area under the blood glucose curve (AUC) was reduced in SG-compared to sham-operated mice (SG, n=4; sham, n=4, AUC $^{**}p= 5.25\times10^{-3}$, two-tailed Welch's t-test). **f**, GLP-1 levels were increased in mice post-SG compared to post-sham (n=11 per group, $^{**}p=3.00\times10^{-3}$, two-tailed Welch's t-test). All data are presented as mean ± SEM.

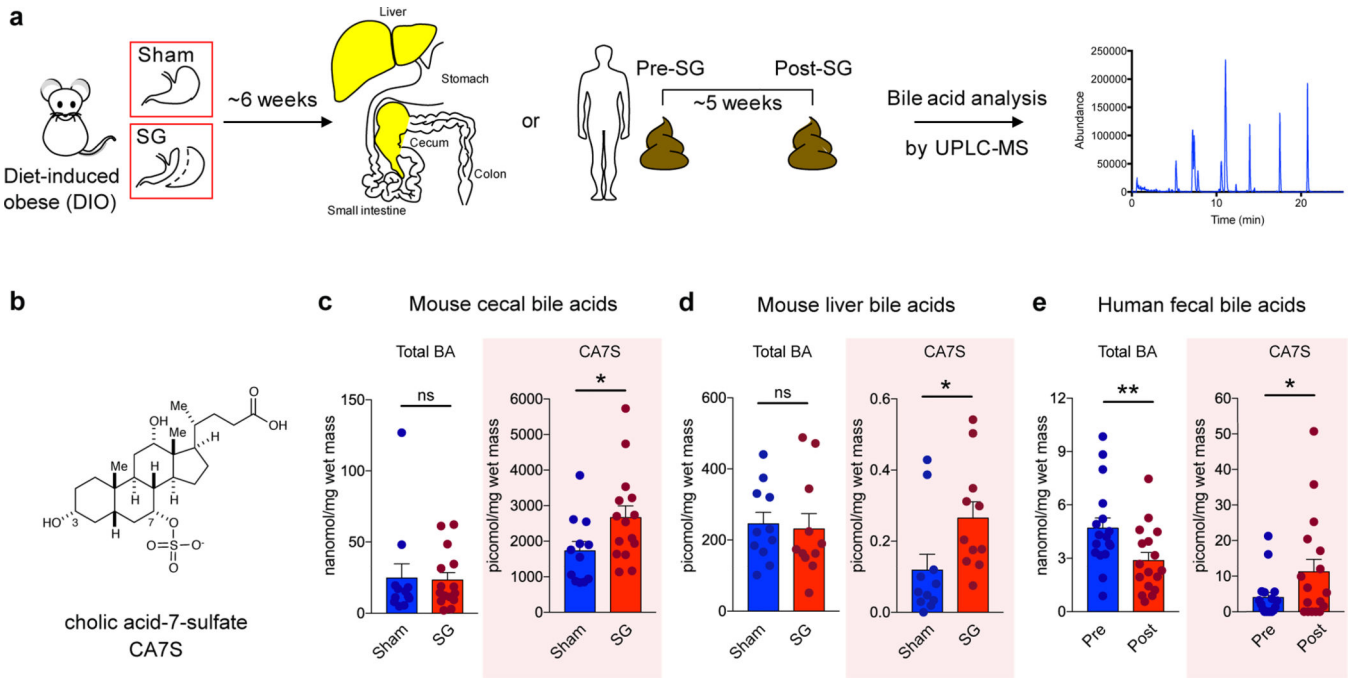

Figure 2. The BA metabolite cholic acid-7-sulfate (CA7S), is increased in mice and humans following SG

a, Schematic of sample collection followed by BA profiling using UPLC-MS. For mice, livers and cecal contents were collected from fasted sham or SG mice 6 weeks post-op. For humans, a pre-operative stool sample was compared with a post-operative sample collected a median of 36 days after surgery. **b**, Structure of CA7S (**1**). **c**, CA7S was increased in cecal contents of SG mice, while total BA (BA) concentrations did not differ between SG and sham mice (sham, n=12, SG, n=15, total BAs (BA) not significant (ns) p=0.90, CA7S *p=0.03, two-tailed Welch's t-test). Note that 1 picomol BA/mg wet mass is approximately equivalent to 1 μM. **d**, CA7S was increased in livers of SG mice (SG, n=11; sham, n=11, total BAs (BA) not significant (ns) p=0.55, CA7S *p=0.03, two-tailed Welch's t-test). **e**, CA7S in human feces was increased post-SG compared to pre-surgery (n=17 patients, total BAs (BA) **$p=1.00\times10^{-3}$, CA7S *p=0.01, two-tailed paired t-test).

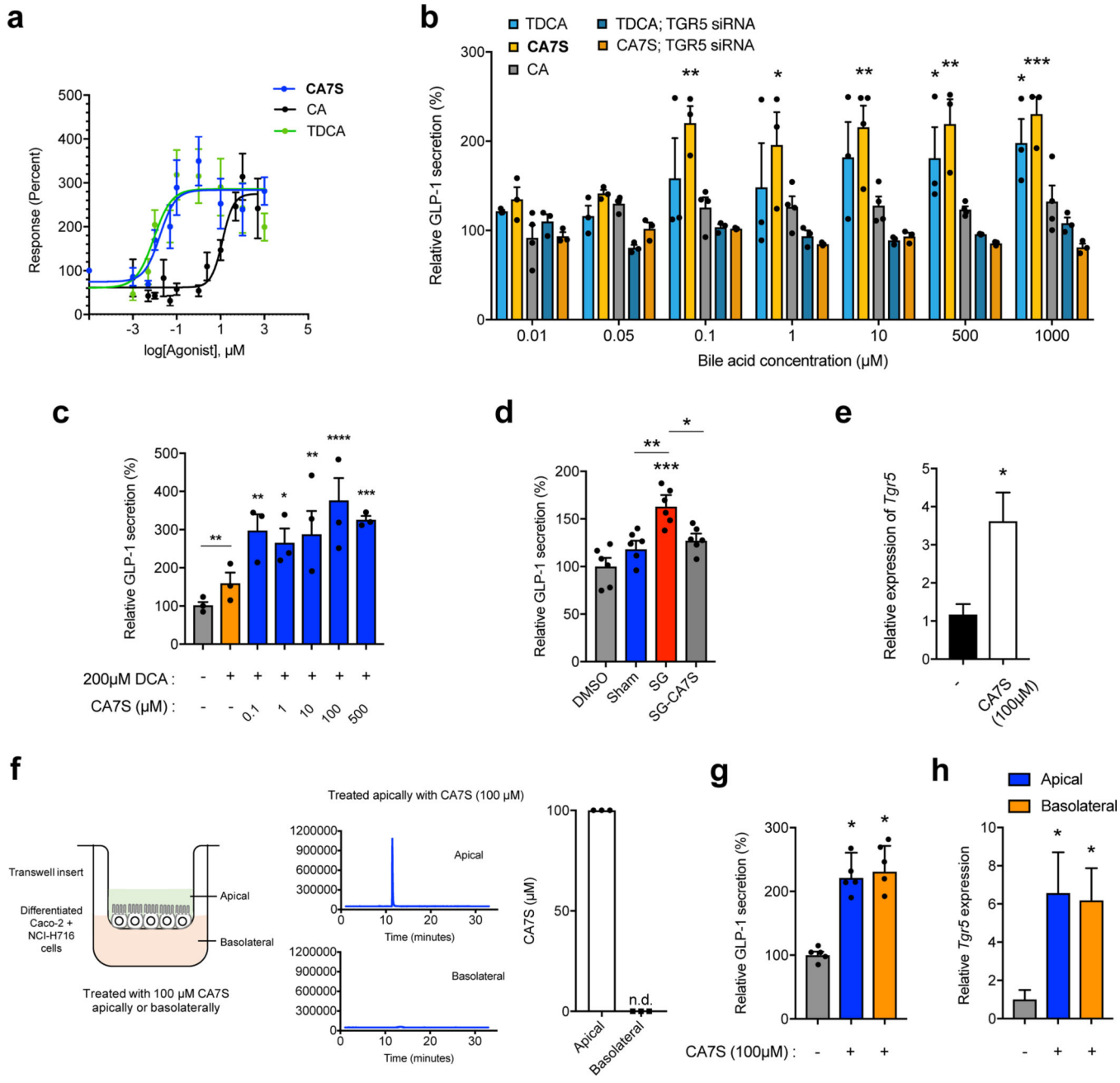

Figure 3. CA7S activates TGR5 signaling and increases *TGR5* expression

a, Dose response curves for human TGR5 activation in HEK293T cells overexpressing human *TGR5* for CA7S, TDCA, CA (3 biological replicates for CA and TDCA, 6 biological replicates for CA7S, see Supplementary Table 1 for EC_{50} values). **b**, CA7S-induced secretion of GLP-1 in NCI-H716 cells compared to both CA and the known TGR5 agonist, TDCA. siRNA-mediated knockdown of *TGR5* abolished GLP-1 secretion (3 biological replicates for all except 4 biological replicates for CA, data not marked with asterisk(s) are not significant. CA7S 0.1 μM **8.00×10^{-3}, 1 μM *p=0.03, 10 μM **p=2.03×10^{-3}, 500 μM **p=3.00×10^{-3}, 1000 μM ***p=7.00×10^{-4}, TDCA 500 μM *p=0.04, 1000 μM *p=0.02,

one-way ANOVA followed by Dunnett's multiple comparisons test). For qRT-PCR expression analysis of *TGR5* knockdown, see Extended Data Fig. 5b. **c**, CA7S induced secretion of GLP-1 in the presence of a physiologically relevant concentration of DCA (200 μM) (3 biological replicates per condition, DMSO (−) control vs. DCA not significant p=0.28, 0.1 μM CA7S vs. DCA **p=4.90×10^{-3}, 1 μM *p=0.03, 10 μM **p=5.30×10^{-3}, 100 μM ****p=1.00×10^{-4}, 500 μM ***p=7.00×10^{-4}, two-way ANOVA followed by Dunnett's multiple comparisons test). **d**, In vitro pools of BAs mimicking the mean physiological concentrations of SG cecal BAs induced GLP-1 secretion in NCI-H716 cells compared to pools of mean sham cecal BAs. Induction of GLP-1 secretion by the SG cecal BA pool was lost when CA7S was removed from the pool (SG-CA7S) (6 biological replicates per condition, data not marked with asterisk(s) are not significant. DMSO vs. Sham not significant p=0.52, DMSO vs. SG ***p=7.00×10^{-4}, DMSO vs. SG-CA7S not significant p=0.24, Sham vs. SG **p=4.00×10^{-3}, SG vs. SG-CA7S *p=0.03, one-way ANOVA followed by Dunnett's multiple comparisons test). **e**, Quantitative real time PCR analysis of *TGR5* expression in NCI-H716 cells treated with CA7S (4 biological replicates per condition, *p=0.01, two-tailed Welch's t-test. **f**, Schematic of differentiated Caco-2 and NCI-H716 cells grown in transwells and treated with CA7S. Apical treatment of epithelial monolayer with 100 μM CA7S led to undetectable amounts of CA7S in the basolateral chamber as measured by UPLC-MS analysis (3 biological replicates, representative UPLC-MS traces shown). **g**,**h**, CA7S (100 μM) induced GLP-1 secretion (**g**) and *TGR5* expression (**h**) when administered apically or basolaterally to a mixed monolayer of Caco-2 and NCI-H716 cells in a transwell system compared to control (5 biological replicates per condition, (**g**) apical CA7S *p=0.02, basolateral CA7S *p=0.01, (**h**) apical CA7S *p=0.03, basolateral CA7S *p=0.02, one-way ANOVA followed by Dunnett's multiple comparisons test). All data are presented as mean ± SEM.

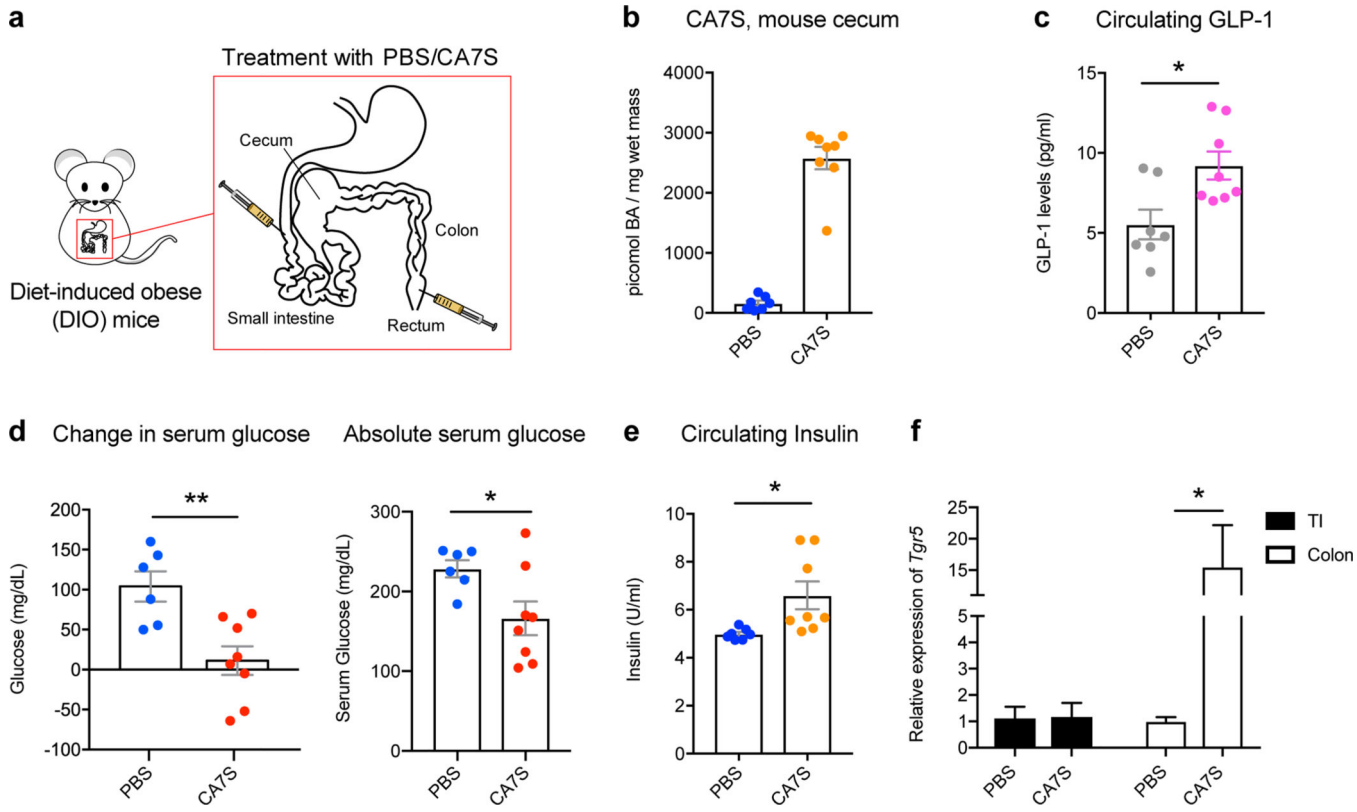

Figure 4. Acute CA7S administration induces GLP-1 and reduces serum glucose levels in vivo

a, Schematic of acute treatment wherein fasted DIO mice were anesthetized and treated with PBS or CA7S via duodenal and rectal catheters. **b**, Concentration of CA7S in mouse cecum 15 minutes after treatment with PBS or CA7S (PBS, n=7; CA7S, n=8 mice). **c**-**e**, CA7S-treated mice displayed increased GLP-1 (**c**), reduced blood glucose levels (**d**), and increased blood insulin levels (**e**) compared to PBS-treated mice. (For **c** and **e**, PBS, n=7; CA7S, n=8 mice, (**c**) *p=0.01, (**e**) *p=0.02, two-tailed Welch's t-test. For **d**, PBS, n=6; CA7S, n=8 mice, **p=4.20×10^{-3}, *p=0.02, two-tailed Welch's t-test). **f**, CA7S treatment in the intestine induced *Tgr5* expression in the colon but not in the terminal ileum (TI) (PBS, n=7; CA7S, n=8 mice, *p=0.03, two-tailed Welch's t-test). All data are presented as mean ± SEM.

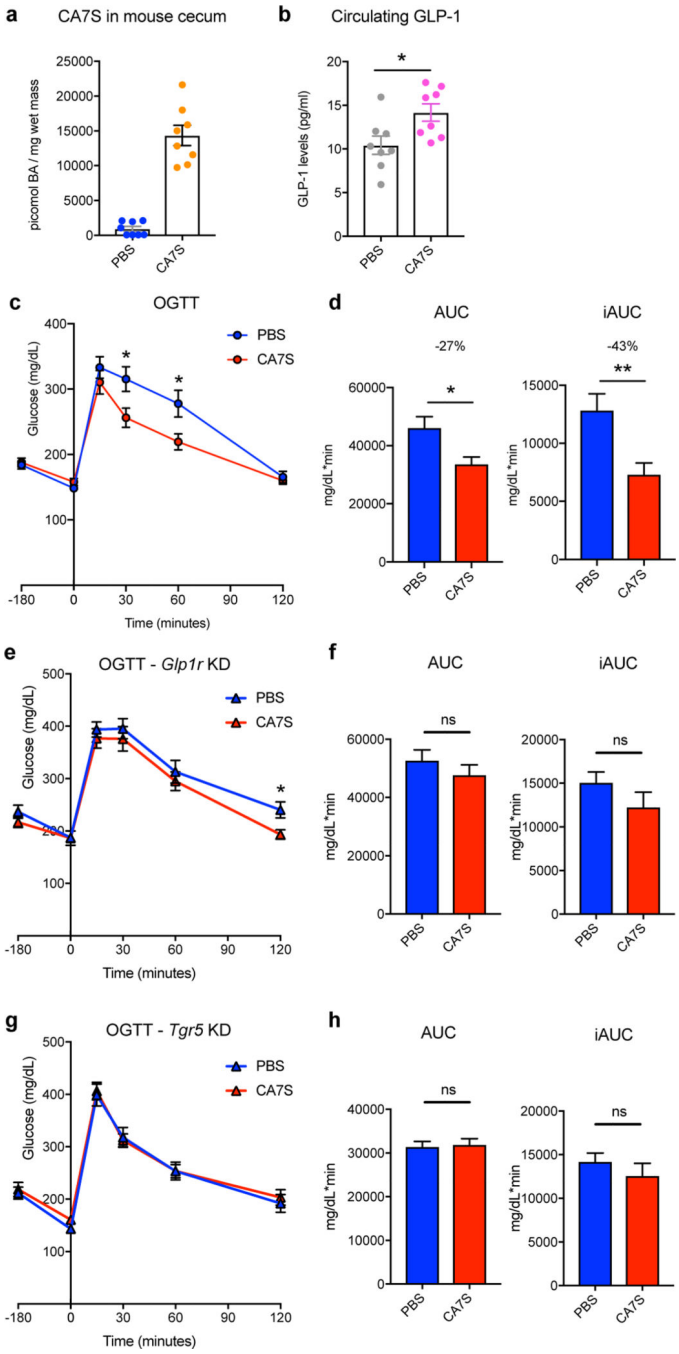

Figure 5. CA7S gavage induces GLP-1 and improves glucose tolerance in vivo via TGR5

a, Concentration of CA7S in mouse cecum 5 hours after PBS or CA7S gavage. **b**, CA7S mice displayed increased GLP-1 levels 5 hours post-gavage. Mice remained fasting for the time between gavage and blood collection for GLP-1 measurement. (For **a** and **b**, n=8 mice per group, **p*=0.02, two-tailed Welch's t-test). **c**,**d**, DIO mice treated with CA7S (100 mg/kg) displayed increased glucose tolerance compared to vehicle-treated mice 3 hours post-gavage as determined by an oral glucose tolerance test (OGTT) (n=11 mice per group). **c**, Glycemic curves during OGTT (data not marked with asterisk(s) are not significant. 30

min *p=0.02, 60 min *p=0.02, 120 min p=0.6, two-tailed Student's t-test). **d**, Corresponding blood glucose AUC and iAUC were significantly reduced in CA7S-treated mice (AUC *p=0.01, iAUC **p=4.00×10^{-3}, two-tailed Welch's t-test). **e**,**f**, On day 3 after treatment with lentiviral shRNA targeting GLP-1 receptor (*Glp1r*), CA7S (100 mg/kg) or PBS was administered, and 3 hours later, an OGTT was performed (n=11 mice per group). **e**, Glycemic curves during OGTT (data not marked with asterisk(s) are not significant. 30 min p=0.53, 60 min p=0.53, 120 min *p=0.02, two-tailed Student's t-test). **f**, Corresponding blood glucose AUC and iAUC were not significantly different in CA7S- or PBS-treated mice in which the *Glp1r* had been knocked down (KD) (ns = not significant, AUC p=0.35, iAUC p=0.20, two-tailed Welch's t-test). **g**,**h**, On day 3 after treatment with lentiviral shRNA targeting *Tgr5*, CA7S (100 mg/kg) or PBS was administered, and 3 hours later, an OGTT was performed (n=9 mice per group). **g**, Glycemic curves during OGTT (data not marked with asterisk(s) are not significant. 30 min p=0.87, 60 min p=0.85, 120 min p=0.52, two-tailed Student's t-test). **h**, Corresponding blood glucose AUC and iAUC were not significantly different in CA7S- or PBS-treated mice in which the *Tgr5* had been knocked down (KD) (ns = not significant, AUC p=0.56, iAUC p=0.97, two-tailed Welch's t-test). For qRT-PCR expression analysis of *Glp1r* and *Tgr5* knockdown in **e-f** and **g-h**, respectively, see Supplementary Figure 9.

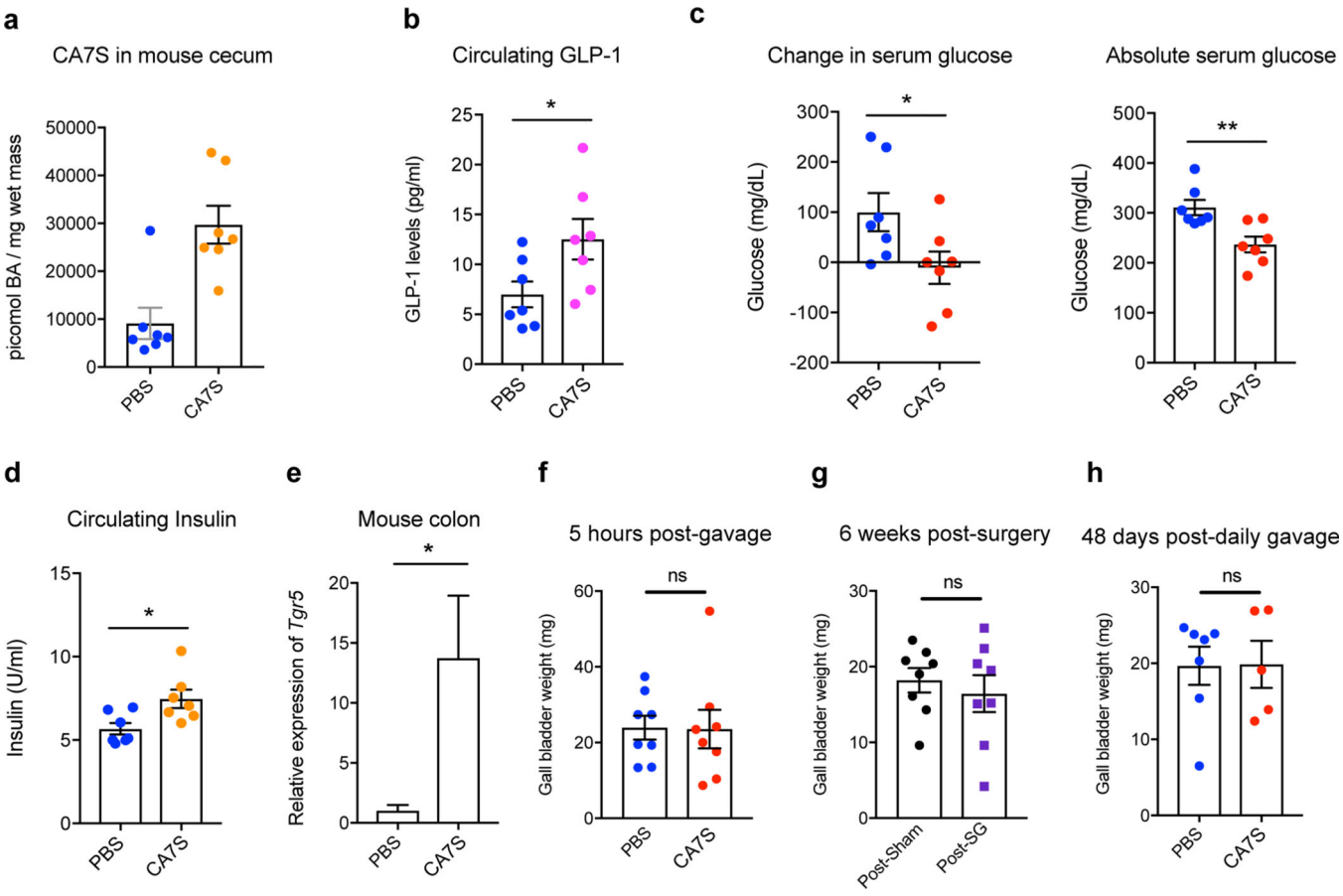

Figure 6. CA7S displays anti-diabetic effects in a chronic setting and does not affect gallbladder filling

a, Concentration of CA7S in mouse cecum at day 48 (n=7 in each group, animals were fasted overnight prior to euthanasia). **b-e**, CA7S-dosed mice displayed increased GLP-1 (**b**), reduced blood glucose levels (**c**), increased blood insulin levels (**d**) and increased *Tgr5* expression in the colon (**e**) compared to PBS-dosed mice. (For **b-e**, n=7 mice in each group), (**b**) GLP-1 levels *p=0.04 (**c**) change in glucose *p=0.04, absolute glucose **p=5.40×10^{-3}, (**d**) insulin levels *p=0.02, (**e**) *Tgr5* expression *p=0.04, two-tailed Welch's t-test). **f-h**, Administration of CA7S did not induce gallbladder filling in mice. For (**f**) Gallbladder weights were measured 5 hours post-gavage with CA7S or PBS (n=8 mice per group, ns=not significant, p=0.95, two-tailed Welch's t-test). For (**g**), gallbladder weights were measured 6 weeks post-sham or post-SG surgery (n=8 mice per group, ns=not significant, p=0.56, two-tailed Welch's t-test). For (**h**), gallbladder weights were measured following 48 days of once-daily gavage with CA7S or PBS (PBS n=7, CA7S n=5 mice, ns=not significant p=0.96, two-tailed Welch's t-test). All data are presented as mean ± SEM.